Charge injection and transport in low-mobility mixed ionic/electronic conducting systems: Regimes of behavior and limiting cases

Thomas J. Mills and Mark C. Lonergan

Charge Injection and Transport in Low-Mobility Mixed Ionic/Electronic Conducting Systems: Regimes of Behavior and Limiting Cases

Thomas J. Mills and Mark C. Lonergan*

Department of Chemistry, The Materials Science Institute, University of Oregon

A comprehensive analysis of a model describing charge carrier injection and transport in light-emitting electrochemical cells (LECs) and related mixed ionic electronic conductors (MIECs) is given. Ions are treated using a modified drift-diffusion transport equation that accounts for volume exclusion effects, and electronic injection is treated using a spatially dependent tunneling mechanism that explicitly accounts for both forward and backward fluxes. Systems containing both one and two mobile ionic species are treated and compared. The unique physics of LECs stem from ionic polarization processes that can lead to field screening and narrowed injection barriers, producing increased electrode exchange currents via tunneling. The latter process promotes the establishment of electronic quasi-equilibrium throughout the double-layer regions and hence promotes bulk-limited conduction. Explicit expressions are given describing the conditions necessary to assume field screening and bulk-limited conduction, which determine the applicability of either traditional semiconductor device models such as Fowler-Nordheim or electrochemical models such as the Nernst equation. Having established these conditions, several distinct regimes of bulk-limited LEC behavior are described. Explicit formulae for the biases delineating these regimes are given as well as formulae for the current in each regime. At low biases, the current generally increases exponentially with bias; the bulk remains field-free, and the transport is predominantly unipolar and diffusive. At high biases the current rises much less rapidly, and bulk transport is bipolar, occurring through a combination of drift and diffusion. The nature of the bulk region in the high-bias regime is markedly different in systems with one and two mobile ionic species. At intermediate biases, space charge effects preferentially drive injection of the minority carrier causing a transition from unipolar to bipolar injection. It is demonstrated that many of the models proposed to describe LECs exist upon a common continuum, and that the major factor separating them is simply the magnitude of the applied bias. This work allows one to estimate at what biases an idealized LEC with particular equilibrium concentrations of ionic and electronic carriers will transition from one mechanism to another. It also aids in conceptually mapping mechanisms and internal details of the system onto each regime of behavior.

I. INTRODUCTION

A number of models have been proposed to explain the underlying physics of light-emitting electrochemical cells (LECs) and related mixed ionic/electronic conductors (MIECs),[1–7] but a broad consensus has not been reached.[8–11] The long-standing debate about which model most accurately describes the steady-state behavior of these devices is very well known in the literature.[12–15] Much of the debate has centered on the electrostatic potential profile.[16–19] However, the potential profile can be difficult to measure and particularly to interpret, due in part to an incomplete appreciation of the full range of behavior exhibited by the basic drift-diffusion/Poisson transport system. A number of papers exploring simulations of special cases of this system have appeared,[1–7] but they have not had sufficient scope to clearly demonstrate the conditions under which each is valid. This problem is compounded by the general lack of analytical results regarding this system in the literature, for without these it can be difficult to make definitive statements.

We aim to assist in rectifying this situation by showing that the existing models are essentially various limiting cases upon a continuum of device behaviors. This notion has been suggested by Smith[2] and deMello[7] and more recently by Pingree et al.[16] and Reenen et al.,[19] but it has not been fully quantified. We identify some of these limiting cases and under what conditions they are valid. We show how to obtain approximate expressions for the current as a function of bias and other system parameters, the biases at which each limiting regime transitions into another, and that the expressions obtained are consistent with simulations. By showing how previous models are interrelated, and that they all grow out of the same physics and the same basic set of equations, we hope that one result of this work will be to direct attention to the question of what is missing from the basic set of "parent" equations that is needed to completely explain the experimental data.

We analyze steady-state MIECs with ion-blocking electrodes using a physical and mathematical formulation which is mostly consistent with previous simulation and analytical work,[1–7] and it appears to be generally agreed upon that the basic drift-diffusion/Poisson equations are at least an acceptable approximation of reality. Results are reported for systems with one mobile ionic species, as might represent a conjugated polyelectrolyte or ionomer,[20–22] and two mobile ionic species, as might represent a semiconductor-salt blend.[1,23] The possibility that there exists a maximum saturation value for the ion concentration is also considered, as would arise from simple finite volume constraints.[37] The inclusion of systems with only one mobile ionic species and constraints on the ion concentrations leads to saturation and depletion effects that are not apparent in more widely studied systems with two mobile ionic species and unconstrained ion concentrations.

Though it may form a good basis for understanding, we emphasize that we do not present the model herein as a complete, definitive description of MIEC physics. In particular, one would expect the high degree of disorder present in many of these systems to have a strong effect on both electronic and ionic transport. The disorder affects the electronic densities of states leading to effectively concentration and field dependent mobilities/diffusion coefficients,[24,25] and the randomly obstructed nature of the bulk material makes the ion transport effectively a percolation problem rather than simple drift-diffusion.[26,27] While one can to some extent include these effects in the model, that is not only beyond the scope of this work, but it is also a subject which we believe is more appropriately addressed after the basic drift-diffusion model is more fully understood.

It is important to address the question of exactly in what sense the results we present can be considered "correct." We consider our results to be correct only in the sense that one can show that they follow from the model as given; the question of how accurately this model describes real LECs and related MIEC systems remains open. We believe this is important because previous simulation and modeling work has been based on models similar to ours, so a more complete description of its consequences sheds light on previous results, how they are related to each other, and how well the model can describe real devices.

We proceed by presenting our model followed by separate analyses of the ionic, electronic, and mixed ionic/electronic systems. Simulation results are used to illustrate important aspects of the carrier and potential profiles, of the electronic current, and to verify analytical results.

II. MODEL

The model describes an idealized, intrinsic (undoped), semiconducting MIEC sandwiched between ion-blocking metal electrodes. Systems containing both mobile anions and cations as well as those containing only one mobile ionic species are treated. These are referred to as two-ion and one-ion systems, respectively.

A. Notation and basic equations

It is convenient to use a reduced variable system. The physical (unreduced) values of the variables are marked with a superscript $*$. The symbols n^*, ψ^*, μ^*, D^*, and F^* represent the particle density, quasi-Fermi level, mobility, diffusion coefficient, and particle flux. These symbols are used both generally and with the subscripts a, c, h, e indicating quantities associated with anions, cations, holes, and electrons, respectively; occasionally for clarity we will use the subscript s to indicate a specific species. The symbols ϕ^*, V^*, x^*, and L^* represent the electrostatic potential, applied bias, position coordinate, and thickness of the MIEC. The quantities k, $\hbar$, q, m, ε, ε_0, and T are the Boltzmann constant, the reduced Planck's constant, the magnitude of the elementary charge, the effective electronic carrier mass, the relative dielectric constant, the permittivity of free space, and the absolute temperature.

The reduction scheme is

$$x = \frac{x^*}{\lambda} \qquad \phi = \frac{\phi^*}{V_T} \qquad F_s = \frac{\lambda F_s^*}{V_T \mu_s^* \tilde{n}_s^*} \qquad n_s = \frac{n_s^*}{\tilde{n}_s^*} \tag{1}$$

where $V_T = kT/q$ is the thermal voltage and $\lambda = \sqrt{kT\varepsilon\varepsilon_0/q^2\tilde{n}_{\text{ion}}^*}$ is the ionic Debye length, where $\tilde{n}_{\text{ion}}^*$ is the equilibrium ionic density in the isolated MIEC. For the ions, $\tilde{n}_s^* = \tilde{n}_{\text{ion}}^*$, and for the electronic carriers $\tilde{n}_s^*$ is the equilibrium density of the carrier at the electrode where it is injected. As with ϕ, V is scaled by the thermal voltage, and ψ by the thermal energy kT. We will use the notation $f' \equiv \partial f/\partial x$.

The model consists of Poisson's equation,

$$\phi'' = n_a - n_c + (\tilde{n}_e^*/\tilde{n}_{\text{ion}}^*)n_e - (\tilde{n}_h^*/\tilde{n}_{\text{ion}}^*)n_h \tag{2}$$

coupled to continuity and flux equations for each species. Generally, because of material disorder, the mobilities and diffusion coefficients may be functions of n, ϕ, and their derivatives,[24,28] but in this work we will assume constant values for both and assume the Einstein relation; in the system of reduced variables this means that $\mu = D$. For ions, the continuity and flux equations are

$$\frac{\partial n}{\partial t} = -F' \tag{3}$$

$$F = -z\phi'n(1 - n/\hat{n}) - n' \tag{4}$$

Here, $z = \pm 1$ is the sign of the charge on the ion, and $\hat{n}$ is its maximum density. The form of the flux equation used here is an extension of the simple drift-diffusion model that takes into consideration the geometric constraint on the number of particles allowable in a given volume, due to finite particle size (see Appendix A 1).

The analogous equations for the electronic species are

$$\frac{\partial n}{\partial t} = -F' - \zeta' \tag{5}$$

$$F = -z\phi'n - n' + \tau \tag{6}$$

The function ζ' is the recombination term, and the function $\tau(x)$ gives the tunneling flux passing between the electrode and the material through any given location x. In some treatments, the tunneling flux is implemented as a boundary condition,[19,29] but in this work, we explicitly treat the spatial dependence of the tunneling process throughout the interfacial regions.

The boundary conditions introduce two parameters: the applied bias V and the active layer thickness L. The electrodes are located at $x = 0$ and $x = L$. The boundary conditions are implemented by requiring that the Fermi levels of the electrodes differ by V, and by setting the boundary fluxes $F(0)$ and $F(L)$. We define the electrode at $x = 0$ as the cathode and $V \equiv \psi_e(\text{anode}) - \psi_e(\text{cathode})$; hence $V > 0$. The electrodes are considered to be ion-blocking, so $F(0) = F(L) = 0$ for the ions; the boundary fluxes for the electronic species will be defined later. We assume that the action of applying a bias across the two electrodes gives rise to thin charged layers on the inner surfaces of the electrodes; these produce fields at the boundaries that are consistent with the voltage difference V. We assume that these charged layers do not affect our calculations in any other way.

Throughout this work we will show figures displaying simulated data for specific systems. To reduce the parameter space somewhat, we will take $T = 25°\text{C}$, $\varepsilon = 5$, and $L^* = 100\,\text{nm}$.

B. The electronic model

We assume that the MIEC behaves as an ideal intrinsic semiconductor; specifically, a nearly-free electron model is employed. Image-charge effects are neglected. In this section we derive flux expressions that serve as boundary conditions for the electronic carriers and provide the tunneling terms τ. For clarity, we present these expressions for electron transfer at the cathode/MIEC interface. In our presentation and discussion of the electronic model, we take $\phi(0) = 0$. Each flux expression involves two terms: one for ingoing (i.e. from electrode to MIEC) carriers (injection) and another for outgoing carriers (ejection).

Defining Δ_e to be the magnitude of the difference between the electrode Fermi level and the conduction band edge energy at the electrode interface, we have $\tilde{n}_e^* = N_C e^{-\Delta_e}$, where N_C is the effective density of states in the conduction band. We define $\delta \equiv \tilde{\psi}_e(\text{anode}) - \tilde{\psi}_e(\text{cathode})$ where $\tilde{\psi}_e$ indicates the Fermi levels of the isolated electrodes. Upon contacting the isolated electrodes to the MIEC, the interchange of charge that occurs in order to bring the system to equilibrium requires that $\phi(L) - \phi(0) = V + \delta$. The quasi-Fermi level inside the MIEC is defined as $\psi_e = -\phi + \ln n_e$, which is equal to 0 at equilibrium.

1. Flux equation

Charge injection is treated using a standard model of a form that has been widely employed in developing classical semiconductor[30,31] and electrochemical theories.[32] In our notation the expression for flux transferred between the electrode and the material is

$$F_{\text{tr}}(\epsilon_c) = \frac{e^{\Delta_e}}{\lambda_F} \int_{\epsilon_c}^{\infty} \kappa_e(\epsilon_x) \int_{\epsilon_x}^{\infty} f_1(\epsilon) - f_2(\epsilon) \, d\epsilon \, d\epsilon_x \tag{7}$$

where ϵ is the total electronic kinetic energy, ϵ_x is the x-component of the electronic kinetic energy, $\epsilon_c = \Delta_e - \phi$ is the potential energy of the electrons at the conduction band edge, $\lambda_F = \mu_e^* \sqrt{2\pi mkT}/q\lambda$ is the effective mean free path, κ_e is the tunneling probability function, f_1 is the electron energy distribution function for the electrode, and f_2 is the distribution for the MIEC. In full generality, these are Fermi-Dirac distributions; however, we will take f_2 to be a Boltzmann distribution.

Here, $F_{\text{tr}}(\epsilon_c)$ represents the flux of electrons whose energies are greater than or equal to ϵ_c transferred between the electrode and the material. If ϵ_c is taken to be the band edge energy at a position well inside the material where the tunneling flux is effectively zero, then $F_{\text{tr}}(\epsilon_c)$ becomes the total injected electronic flux $F_e(0)$, which is the total flux passing through the electrode/MIEC interface at $x = 0$; this therefore serves as the electronic boundary condition. Because some portion of this flux is due to the thermal emission process at the interface and the rest is due to the spatially dependent tunneling process, it is written with two contributions, $F_e(0) = F_{\text{TE}} + \tau_e(0)$.

2. Thermal emission

The classical thermal emission model for transfer between metal and semiconductor[33] can be derived easily from the flux equation by assuming that transfer occurs between all particles exceeding the band edge energy strictly at $x = 0$; this implies that $\kappa_e = 1$ and $\epsilon_c = \Delta_e$ (i.e., $F_{\text{TE}} = F_{\text{tr}}(\Delta_e)$). Applying Boltzmann statistics one obtains

$$F_{\text{TE}} = \frac{e^{\Delta_e}}{\lambda_F} \int_{\Delta_e}^{\infty} \int_{\epsilon_x}^{\infty} e^{-\epsilon} - e^{-\epsilon + \psi_e(0)} \, d\epsilon \, d\epsilon_x = \frac{1 - n_e(0)}{\lambda_F} \tag{8}$$

where we have used $n_e(0) = e^{\psi_e(0)}$. This gives the thermal emission contribution to the boundary condition for $F_e(0)$. By the same considerations, the thermal emission flux at the other electrode is $(n_e(L) - 1)/\lambda_F$.

3. Tunneling

We take the tunneling probability function to be

$$\kappa_e = \exp\left[-\lambda_\nu^{-1} \int_0^x \sqrt{\phi(x) - \phi(y)} \, dy\right] \tag{9}$$

which is the WKB approximation giving the probability of tunneling through a given potential barrier, where $\lambda_\nu = \hbar/\lambda\sqrt{2mkT}$ is a reduced de Broglie wavelength.[34] We evaluate the supply functions, and we will write $\beta(\epsilon_x) = e^{\Delta_e}\int_{\epsilon_x}^\infty f_1(\epsilon)\,d\epsilon$ for the electrode supply function in order to preserve generality (so that one may use a Fermi-Dirac distribution if necessary). The tunneling flux then becomes

$$\tau_e(\epsilon_c) = \lambda_F^{-1} \int_{\epsilon_c}^{\Delta_e} \kappa_e(\epsilon_x) \left(\beta(\epsilon_x) - e^{\Delta_e + \psi_e - \epsilon_x}\right) d\epsilon_x \tag{10}$$

An unclear aspect of the flux expression to this point is that it incorporates both energy and position-dependent quantities, yet it is phrased as an integral over energy. The approach here is to note that tunneling is inherently a spatially dependent process due to the fact that an electron cannot emerge in a region in which it would have negative kinetic energy. We hereby assume that all electrons capable of emerging at a particular location do so; that is, all particles of energy ϵ_x emerge at the location where $\epsilon_x = \epsilon_c$. We then rewrite the integral in terms of the spatial coordinate x, where the integration variable x is taken to be the location at which $\epsilon_x = \epsilon_c$, and hence the location at which all electrons with energy ϵ_x emerge into the system (or, equivalently, from which they are expelled from the system back into the electrode).

By these considerations, upon noting that $d\epsilon_x = d\epsilon_c = -d\phi = -\phi'\,dx$ and that we must have $\tau_e \sim 0$ far from the electrode, the tunneling flux may be written explicitly as a function of x,

$$\tau_e(x) = \lambda_F^{-1} \int_x^{x_1} \phi' \kappa_e \left(\beta(\phi) - n_e\right) dx \tag{11}$$

where the integrand is negligibly small at x_1. This is the x-dependent tunneling flux function that appears in the transport equation (6). A conceptual illustration of Eq. (11) is shown in Fig.1.

4. Recombination

Recombination depends strongly on the charge density profiles. This work investigates only a simple second-order (Langevin) model,[35]

$$\zeta_s' = k_s n_e n_h \tag{12}$$

The variable reduction scheme we have chosen requires that $k_s = (\lambda^2/V_T\mu_s^*)(\tilde{n}_e^*\tilde{n}_h^*/\tilde{n}_s^*\tilde{n}_{\text{ion}}^*)k^*$, where k^* is the electron/hole recombination constant. Note that, with low mobilities, k_s becomes large, reflecting the fact that the lower rate of transport increases the likelihood of recombination. If we define $\zeta_e(0) = \zeta_h(L) = 0$, then the function $\zeta_s(x)$ represents the total density of recombining particles per unit time between x and the injection electrode.
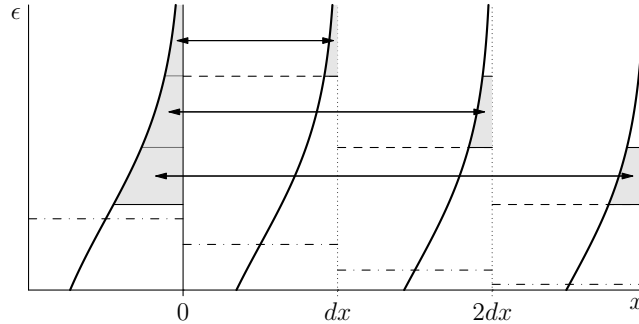

FIG. 1. A conceptual illustration of the electronic injection mechanism. In each slice of width dx, the solid lines represent the energy distributions f, the dash-dotted lines represent the (quasi-) Fermi levels ψ_e, the dashed lines represent the potential energy $-\phi$, the shaded regions represent the supply functions, and the arrows represent the bidirectional flux between the electrode (shown to the left of $x = 0$) and each slice. These fluxes are proportional to the difference in the shaded areas, each weighted by the factor κ_e/λ_F. Transfer between the electrode and the first slice represents the thermal emission boundary condition, and transfer further into the device represents the spatially-dependent tunneling process.
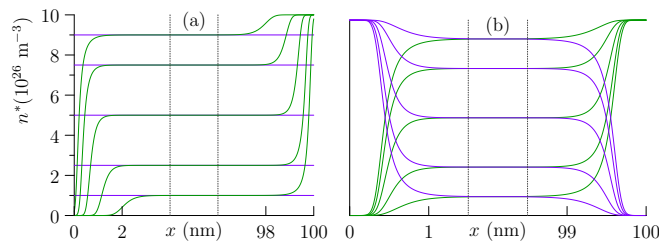
FIG. 2. Ion profiles for (a) one-ion (mobile anions) and (b) two-ion systems, where $V^* = 1$ V, $L^* = 100$ nm, $\hat{n}_a^* = \hat{n}_c^* = 10^{27} \mathrm{m}^{-3}$ and $\tilde{n}_{\mathrm{ion}}^* = 1, 2.5, 5, 7.5, 9 \cdot 10^{26} \mathrm{m}^{-3}$ ($\hat{n} = 10, 4, 2, 4/3, 10/9$), with n_a shown in green and n_c in purple. This figure shows the depletion and saturation behavior and the symmetry between systems capped at $\hat{n}$ and those at $\hat{n}/(\hat{n} - 1)$. Note the thinner double layers in the two-ion system.

C. Simulations

The model presented thus far forms the basis for our simulations, which are constructed using finite-difference approximations to the Poisson, transport, tunneling flux, and recombination equations (Eqs. (2)-(6), (11), and (12)), using thermal emission (Eq. (8)) and tunneling (Eq. (11)) as boundary conditions. To obtain steady-state results, the simulations were run until there was a negligible change in the system variables. A more detailed description of the simulation methods can be found in the supporting information.[36]

The simulations were very useful as a guide to understanding qualitative system behavior and quantitative verification of analytical results.

III. IONIC SUBSYSTEM

In this work, we investigate MIEC systems with relatively large densities of ions. In such systems, the ions play a central role in determining the electrostatic potential and hence the details of electronic carrier injection and transport. Therefore, in order to understand the electronic behavior of these systems, it is imperative to have a good understanding of the behavior of the ions. To this end, we begin by analyzing the steady-state properties of purely ionic systems.

In this section, we first give the ion distributions in terms of the electrostatic potential ϕ. Next, we delineate the conditions under which the ions will screen the electric fields induced by the electrodes. Finally, we provide expressions for the potential drops across the ionic layers and the boundary fields in screened systems. These quantities will later be related to the electronic charge densities and fluxes in Sec. V.

The results in this section are derived from Eqs. (2) – (4) with $n_e = n_h = 0$ and $F_s(0) = F_s(L) = 0$ for $s = a, c$. In analyzing purely ionic systems, we let $\delta = 0$, so that $\phi(L) - \phi(0) = V$. Steady-state analytical results are obtained by setting $\partial n/\partial t = 0$.

There exists a certain symmetry between systems with $\hat{n} > 2$ and those with $\hat{n} < 2$. For analytical simplicity, we will hereafter assume that $\hat{n} > 2$, but the results for $\hat{n} < 2$ can be obtained by exploiting the symmetry of the system. This symmetry allows the problem to be recast in terms of ion "holes" through the use of the transformations $n \leftarrow (\hat{n} - n)/(\hat{n} - 1), \hat{n} \leftarrow \hat{n}/(\hat{n} - 1), x \leftarrow L - x, F \leftarrow F/(\hat{n} - 1), z \leftarrow -z$, which leave the transport equation unmodified. This shows that ion holes behave in the same way as do ions of opposite charge, reflected about the axes $x = L/2$ and $n = \hat{n}/2$.

The results in this section rely on a method of integrating Poisson's equation. See Appendix A 2 for details.

A. Ion distributions

The results of steady-state simulations of both one- and two-ion systems with different values of $\tilde{n}_{\mathrm{ion}}^*$ are shown in Figures 2 and 3. Qualitatively, the behavior of the mobile ions is relatively straightforward; ions move away from one electrode, forming the *depletion region*, and towards the other electrode, forming the *accumulation region*. Both of these are called *double layers*. The symmetry about $\hat{n} = 2$ is readily apparent in Fig. 2. In the two-ion system, the accumulation region for one sign of ion will overlap with the depletion region of the other sign of ion. Provided the length of the device is sufficiently large, there exists a *bulk region* between the depletion and accumulation regions in which n is nearly constant.
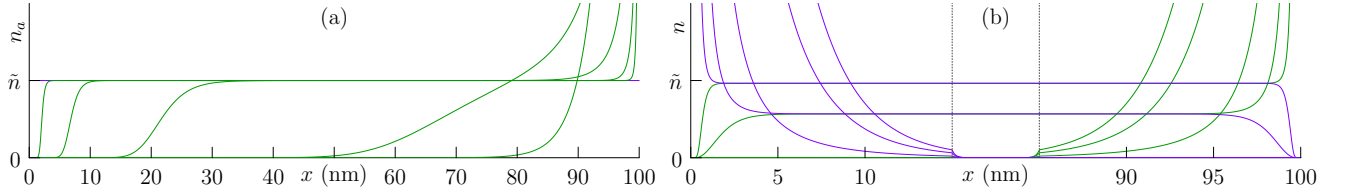
FIG. 3. Ion profiles for (a) one-ion (mobile anions) and (b) two-ion systems with $\tilde{n}^*_{\text{ion}} = 10^{26}, 10^{25}, 10^{24}, 10^{23}$, and 10^{22} m^{-3} (other parameters are the same as in Fig. 2), with n_a shown in green and n_c in purple. As the ion content is decreased, the depletion and accumulation regions become wider until all of the ions are pushed into the accumulation layers. In two-ion systems, the bulk becomes depleted of ions.

In general, the depletion and accumulation regions may contain two parts: a *compact region* in which the concentration approaches 0 (*fully depleted*) or $\hat{n}$ (*saturated*), and a *diffuse region* in which the concentration transitions from its bulk value either to that in the compact layer - if it exists - or to the concentration at the electrode surface. If the accumulation region contains a compact region, the device is said to be in the *saturation limit*; if its diffuse region extends to the electrode, the device is said to be in the *diffuse limit*. In section III C, we show that for one-ion systems, the saturation limit occurs when $V > \hat{n}$ and for two-ion systems, it occurs when $V > 2\ln\hat{n}$.

Eqs. (3) and (4) can be solved to yield

$$n = \frac{\hat{n}}{1 + (\hat{n}/n_B - 1)e^{z(\phi - \phi_B)}} \tag{13}$$

This solution is referenced to the bulk concentration n_B and potential ϕ_B, defined as the concentration and potential at the location where $n_a = n_c$.

Note that the distribution (13) arises as the equilibrium solution to the transport equation (4). This distribution is the same as given, e.g., by Eq. (3-2) in Eigen and Wicke,[37] and is based on the same physical considerations. As $\hat{n} \to \infty$, it degenerates to the Boltzmann distribution $n = n_B e^{-z(\phi - \phi_B)}$.[38]

Eq. (13) gives the ion concentration as a function of ϕ; Poisson's equation must then be solved to obtain $\phi(x)$ and hence $n(x)$. Only the diffuse limit of the two-ion system can be solved exactly. Some analytical approximations can be made. For instance, $\phi(x)$ will be approximately quadratic in any fully depleted or saturated region because the excess charge density in these regions is nearly constant, and it decays exponentially into the bulk region. We will use a quadratic approximation for ϕ later, for example, when deriving the conditions for electronic quasi-equilibrium in Sec. V A.

B. Field screening

An important property of an ionic system is whether or not it is *screened*. This property can be defined by the existence of a bulk region that is practically free of an electric field. If there are "enough" ions available to polarize at the electrodes, they will "screen" the fields induced there by the applied bias. We write ϕ'_B for the bulk field; specifically, ϕ'_B is the value of ϕ' at the location where $n_a = n_c$. The field is said to be screened when ϕ'_B is sufficiently small. Prior analyses have shown that the screening condition is violated particularly when decreasing the ion content; essentially, the system will be screened if the device is long enough relative to the Debye length.[9,39] Here we make this heuristic quantitative in the context of the present model by showing how many Debye lengths is "long enough."

A fairly tight upper bound on ϕ'_B can be obtained directly from Poisson's equation. Eq. (2) can be rewritten to relate L and the ion distributions to ϕ'_B,

$$\int_{\phi(0)}^{\phi(L)} \frac{d\phi}{\sqrt{\phi'^2_B + 2\int_{\phi_B}^{\phi} n_a(\Phi) - n_c(\Phi)\, d\Phi}} = L \tag{14}$$

As detailed in Appendix A 3, an upper bound on Eq. (14), with mobile ion distribution(s) given by Eq. (13), is found by defining the boundaries of the compact, diffuse, and bulk regions, and then bounding the integrand separately in each region. The inequality obtained from bounding Eq. (14) is then solved for ϕ'_B,

$$\phi'_B < e^{-\frac{1}{2}\sqrt{\bar{n}}(L - w_{\text{cp}} - w_{\text{df}} - \xi)} \left(\sqrt{\bar{n}} + \frac{2}{L - w_{\text{cp}} - \xi} \right) \tag{15}$$

where $\bar{n}$ is a concentration parameter, $\hat{n} < 10^6$, and ξ is a small parameter necessary to maintain the upper bound. Note that the length occurring in the exponent is the effective width of the bulk region.

For one mobile ionic species, $n_B = 1$, $\bar{n} = 1 - 1/\hat{n}$, $\xi < 0.77$, and when the accumulation region is saturated,

$$w_{\text{cp}} = \bar{n}^{-1}\sqrt{2}\sqrt{\bar{n}V - \ln(\hat{n} - 1) + \hat{n}\ln\bar{n}} \tag{16}$$

$$w_{\text{df}} = \bar{n}^{-1/2}\ln(4(\hat{n} - 1)\ln\bar{n}^{-1}\ln\hat{n}) \tag{17}$$

If the accumulation region is not saturated, $w_{\text{cp}} < \sqrt{2V}$ and $w_{\text{df}} < 4$.

The exponential in Eq. (15) will be small as long as the width of the bulk region is appreciable. However, ϕ'_B will begin to increase rapidly as this width approaches 0, marking the loss of screening. By comparing the dominant term of Eq. (16) to L, it is then easy to obtain the approximate screening condition for saturated systems

$$V < \frac{\bar{n}}{2}L^2 \tag{18}$$

where $\bar{n}$ is replaced with 1 in the diffuse limit.

The situation for two-ion systems is more complicated because the bulk may become partially depleted of ions (see Fig. 3) while remaining electroneutral; the bulk concentration n_B will decrease with increasing bias. In the diffuse limit, it is possible to solve Poisson's equation exactly. With this solution one can show (see Appendix A 4) that a two-ion system will reach saturation before loss of field screening as long as $\hat{n} \ll L^4$; this inequality is expected to hold for most realistic systems.

We therefore continue with the saturation limit. Here, we have $\bar{n} = n_B(2 - n_B/\hat{n}_a - n_B/\hat{n}_c)$, $\xi = \ln(\hat{n}_a\hat{n}_c/n_B^2)/49 < V/49$, and

$$w_{\text{cp}} = \sqrt{2}\sqrt{\left(\hat{n}_a^{-1} + \hat{n}_c^{-1}\right)\left(V - \ln(\hat{n}_a\hat{n}_c/n_B^2)\right)} \tag{19}$$

$$w_{\text{df}} = \bar{n}^{-1/2}\ln(4\ln(\hat{n}_a/n_B)\ln(\hat{n}_c/n_B)) \tag{20}$$

If n_B, and hence $\bar{n}$, is not close to zero, the exponential of Eq. (15) will be small as long as the bulk region is appreciable. However, when n_B becomes on the order of $1/L^2$, the terms in the exponent will all become small except for the diffuse layer term $\sqrt{\bar{n}}w_{\text{df}}/2$, which continues to rise with increasing bias, marking the loss of screening. This shows that there are two mechanisms that can cause the loss of field screening: the compact layer widths can approach L while n_B is not small, and the decrease of n_B can cause the diffuse layers to become very wide. In both cases, as with one mobile ionic species, the loss of screening occurs when the effective bulk width approaches zero.

To estimate when n_B becomes small, we neglect the diffuse layers (abrupt-layer approximation) and apply conservation of ionic charge to get

$$n_B \approx \frac{L - \frac{\hat{n}_a\hat{n}_c}{\hat{n}_a + \hat{n}_c}w_{\text{cp}}}{L - w_{\text{cp}}} \tag{21}$$

Setting this expression to zero and using the dominant term of Eq. (19) gives the approximate condition $V \approx (L^2/2)(1/\hat{n}_a + 1/\hat{n}_c)$ for when n_B becomes small. Comparing L to w_{cp} in a similar way shows that the compact layers overtake the device length when $V \approx (L^2/2)(1/\hat{n}_a + 1/\hat{n}_c)^{-1}$. From this, we see that the bulk will become depleted before the compact layers get too large (unless $\hat{n}_a = \hat{n}_c = 2$, in which case these occur in concert). Hence, an approximate screening condition for the two-ion case is

$$V < \frac{1}{2}\left(\frac{1}{\hat{n}_a} + \frac{1}{\hat{n}_c}\right)L^2 \tag{22}$$

It is apparent from comparing Eqs. (18) and (22) that two-ion systems cannot screen the electrode fields as effectively as one-ion systems because of the depletion of ions from the bulk. The onset of this depletion with voltage is tempered by ion saturation. Systems that can accommodate greater concentrations of ions in their saturation layers lose field screening at lower voltages. Also recall that L is given in units of λ, and hence, the voltage at which field screening is lost increases with increasing $\tilde{n}^*_{\text{ion}}$ in both one- and two-ion systems. The compact and diffuse layers are shown in Fig. 4.

The remainder of this work will provide results for systems that satisfy the ionic screening condition. We will assume for two-ion screened systems that $n_B \approx 1$.
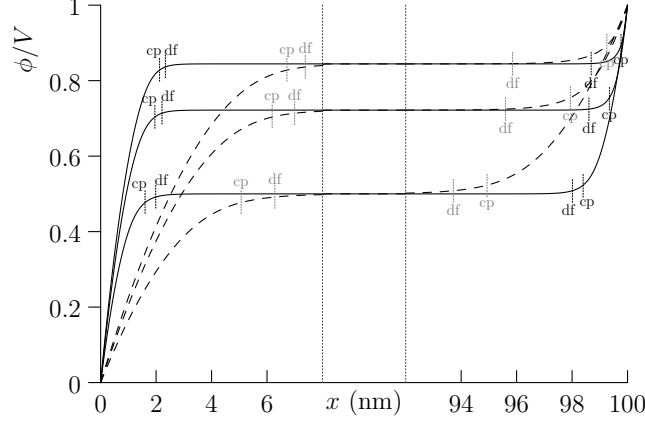
FIG. 4. Simulated electrostatic potential profiles for a one-ion system with $V^* = 1\,\mathrm{V}$, $\hat{n} = 10, 4, 2$, and $\tilde{n}_{\mathrm{ion}}^* = 10^{26}\,\mathrm{m}^{-3}$ (solid lines), $\tilde{n}_{\mathrm{ion}}^* = 10^{25}\,\mathrm{m}^{-3}$ (dashed lines). Note the dependence of the double-layer potential drops on $\hat{n}$; their values at the two electrodes are equal for $\hat{n} = 2$, whereas a larger fraction of the applied bias drops at the depletion layer side extending from $x = 0$ as $\hat{n}$ increases. Note also the larger double-layer widths with fewer ions. The effective edges of the compact and diffuse layers are marked with cp and df, respectively, and calculated according to the considerations of Sec III B. Note that the diffuse layers are larger in the accumulation regions.

C. Double Layer Potential Drops and Boundary Fields

Figure 4 shows representative electrostatic potential profiles for screened one-ion systems obtained from simulations. Though the model does not in general admit an explicit solution for $\phi(x)$, we will derive expressions for the potential drops across the double layers and for the boundary field ϕ_0' in screened systems. This will become important later because the electronic behavior depends critically on these values, but it is not particularly sensitive to the precise form of $\phi(x)$. Note also that ϕ_0' is equal to the total excess charge stored in each double layer. We define x_- and x_+ to be the locations of the edges of the ionic double layers on the cathode and anode side, $\Delta\phi_- = \phi(x_-) - \phi(0)$ to be the potential drop across the double layer on the cathode side, and $\Delta\phi_+ = \phi(L) - \phi(x_+)$ to be the potential drop on the anode side. Because the system is screened, $\phi(x_-) = \phi(x_+) = \phi_B$, and since there is no excess charge in the system, $\phi_0' \equiv \phi'(0) = \phi'(L)$. The potential drops and boundary fields are obtained from Poisson's equation and Eq. (13) (see Appendix A 5).

1. One-ion systems

Under bias, a region depleted of ions forms at the electrode with the same sign of charge as the ions. We will label the potential drop across this region $\Delta\phi_{\mathrm{dep}}$. The ions also accumulate at the other electrode, where there is a drop of $\Delta\phi_{\mathrm{acc}}$. Hence, for mobile anions we have $\Delta\phi_- = \Delta\phi_{\mathrm{dep}}$, and for mobile cations, $\Delta\phi_- = \Delta\phi_{\mathrm{acc}}$. We only give the results for $\Delta\phi_{\mathrm{dep}}$ because $\Delta\phi_{\mathrm{acc}}$ can be obtained by using $\Delta\phi_{\mathrm{dep}} + \Delta\phi_{\mathrm{acc}} = V$.

For screened systems, there is an exact solution,

$$\Delta\phi_{\mathrm{dep}} = \ln\left[\frac{e^{(1-1/\hat{n})V} - 1}{(\hat{n}-1)(1 - e^{-V/\hat{n}})}\right] \tag{23}$$

$$\phi_0' = \sqrt{2}\sqrt{\hat{n}\ln\left[1 + \frac{e^{-\Delta\phi_{\mathrm{dep}}} - 1}{\hat{n}}\right] + \Delta\phi_{\mathrm{dep}}} \tag{24}$$

We take limits of these expressions to more clearly demonstrate the forms of the potential drops and boundary fields. In the saturation limit,

$$\Delta\phi_{\mathrm{dep}} = (1 - 1/\hat{n})V - \ln(\hat{n} - 1) + O\left(e^{-V/\hat{n}}\right) \tag{25}$$

$$\phi_0' = \sqrt{2}\sqrt{(1 - 1/\hat{n})V - \ln(\hat{n}-1) + \hat{n}\ln(1 - 1/\hat{n})} \\ + O\left(e^{-V/\hat{n}}/\sqrt{V}\right) \tag{26}$$

and in the diffuse limit,

$$\Delta\phi_{\text{dep}} = V - \ln V + O\left(e^{-V} + V/\hat{n}\right) \tag{27}$$

$$\phi_0' = \sqrt{2}\sqrt{V - \ln V - 1} + O\left(\sqrt{V}e^{-V} + \sqrt{V}/\hat{n}\right) \tag{28}$$

As can be seen from these expressions and their error terms, the ratio $V/\hat{n}$ determines whether or not the system is saturated. This can be understood readily by investigating the ionic concentration at the accumulation electrode surface. Using Eq. (13) and $\Delta\phi_{\text{acc}} \approx \ln V$, the surface concentration in the diffuse limit is approximately $e^{\Delta\phi_{\text{acc}}} \approx V$. From this, one can see that the system will approach saturation when V approaches $\hat{n}$.

Note that, in order to conserve the ions, an equal amount of excess charge must be stored in the accumulation layer as in the depletion layer. In the limit of $\hat{n} = 2$, the system is symmetric about $x = L/2$, and the excess charge is stored in double layers of equal width. As $\hat{n}$ increases, the charge in the accumulation layer is stored in a region of increasingly narrower width. This results in a smaller potential drop across the accumulation layer (see Fig. 4), which is approximately $V/\hat{n}$ in the saturation limit; in the diffuse limit, this potential drop approaches the relatively small value of $\ln V$.

2. Two-ion systems

In the diffuse limit, or if $\hat{n}_a = \hat{n}_c$, then because of the spatial symmetry of the system, the potential drops will be $\Delta\phi_- = \Delta\phi_+ = V/2$. Before the system becomes saturated, its behavior is very different from the one-ion case because there is no region fully depleted of mobile ions. Instead, both ionic species accumulate in very thin and steep layers near the electrodes. The concentrations at the electrode surfaces are approximately $e^{V/2}$, and hence the ions approach saturation near $V \approx 2\ln\hat{n}$. Note that saturation occurs at much lower biases in the two-ion case because of the exponential rise of the accumulating ions with bias, rather than the linear behavior observed in the one-ion case. We consider further only the saturation limit because the bias at which the system approaches saturation is not at all large for any realistic degree of ion loading.

In the saturation limit, we have

$$\Delta\phi_- = \frac{\hat{n}_a V - \hat{n}_a \ln(\hat{n}_a - 1) + \hat{n}_c \ln(\hat{n}_c - 1)}{\hat{n}_a + \hat{n}_c}$$

$$+ O\left(e^{-\frac{\hat{n}_a}{\hat{n}_a+\hat{n}_c}V} + e^{-\frac{\hat{n}_c}{\hat{n}_a+\hat{n}_c}V}\right) \tag{29}$$

$$\phi_0' = \sqrt{2/(\hat{n}_a + \hat{n}_c)}\left[\hat{n}_a\hat{n}_c(V - \ln(\hat{n}_a\hat{n}_c))\right.$$

$$\left. + \hat{n}_a^2\ln(1 - 1/\hat{n}_a) + \hat{n}_c^2\ln(1 - 1/\hat{n}_c)\right]^{1/2}$$

$$+ O\left(\frac{1}{\sqrt{V}}\left[e^{-\frac{\hat{n}_a}{\hat{n}_a+\hat{n}_c}V} + e^{-\frac{\hat{n}_c}{\hat{n}_a+\hat{n}_c}V}\right]\right) \tag{30}$$

Note that, if one uses the expressions above and employs an abrupt junction approximation to obtain effective double-layer widths (the effective width of a layer is ϕ_0'/ρ, where ρ is the magnitude of the excess charge density in the layer), then requiring that L is greater than the sum of these widths gives a screening condition very similar to that found in Sec. III B.

IV. ELECTRONIC SUBSYSTEM

As one of the main goals of this work is to analyze electronic conduction in low-mobility MIEC systems, we require a framework for describing injection and transport in general electronic systems. Of particular importance are the concepts of injection- and transport-limited conduction. We describe the characteristics of and conditions necessary for these limits, emphasizing their dependence on the electronic mobility, the role of tunneling, and the concept of quasi-equilibrium. In the process, we develop some basic tools for describing carrier profiles and fluxes that we will use later to analyze full MIEC systems. The analysis of this section is conceptually similar to that of metal/semiconductor junctions, such as the combined thermionic-emission/diffusion theory of Crowell and Sze.[40] In this section we will again provide results for electron transfer only.

A. Injection mechanisms and the notion of quasi-equilibrium

Recall the thermal emission flux formula $F_e = (1 - n_e(0))/\lambda_F$. Written in this form, it becomes clear that this mechanism can be understood essentially as basic diffusion across an interface. Note that the limiting form as $n_e(0) \to 0$, $F_e \sim \lambda_F^{-1}$, is equivalent to the ideal backwards-biased Schottky saturation current (this can be seen by moving back to physical variables, *i.e.* $F_e^* = V_T \mu_e^* \tilde{n}_e^*/\lambda\lambda_F = AT^2 N_C e^{-\Delta_e}$ where $A = 4\pi qmk^2/h^3$ is the Richardson constant); here the flux is determined entirely by the injection process.

If λ_F becomes infinitesimal (i.e., when the mobility is very small), then in order for the thermal emission flux to remain finite, the difference $1 - n_e(0)$ must become infinitesimal as well. This limit, $n_e(0) \sim 1$, is equivalent to $\psi_e(0) \sim 0$, or what is the same, the establishment of local quasi-equilibrium between the electrode and the inner material surface. Here, the flux depends on the infinitesimal deviation of $n_e(0)$ from its equilibrium value, and therefore it depends entirely on the transport process.

Similarly, recall the tunneling flux formula $\tau_e(x) = \lambda_F^{-1} \int_x^{x_1} \phi' \kappa_e(\beta(\phi) - n_e)\, dx$. As was the case with thermal emission, it is easy to identify the injection-limited regime, in which n_e is considered negligible throughout the entire injection region ($0 < x < x_1$). The tunneling flux formula in this limit ($n_e \to 0$) gives rise to such models as the Fowler-Nordheim formula. The use of this limit, however, is a drastic assumption because it ignores all coupling of the electrode to the transport processes by ignoring n_e throughout the injection region, consequently ignoring all back-flux. Expressions derived from this limit are therefore not valid when there is a large amount of coupling, as there is when the carrier mobility is small. The importance of back-flux and its effect on carrier injection in organic semiconductors with low carrier mobility has been recognized, but prior treatments have been primarily phenomenological and without the level of rigor afforded to the forward flux.[29,41] It is important to note that we have treated the forward and backward flux equivalently, using the same physics, and in a way that is thermodynamically consistent.

To investigate the low-mobility limit, we may apply the same argument to the tunneling flux $\tau_e(x)$ as we did to the thermal emission flux. If $\lambda_F \to 0$, then we must have $\phi' \kappa_e(\beta - n_e) \to 0$ for τ_e to remain finite. In other words, in any region where $\lambda_F^{-1} \phi' \kappa_e$ is not negligibly small, n_e must approach β. Consequently, as we have assumed n_e to be governed by Boltzmann statistics, then β must be in the Boltzmann limit as well, and hence $\beta \sim e^\phi$, which in turn implies $n_e \sim e^\phi$ in this region. We call this the *quasi-equilibrium region* that has been formed by the tunneling mechanism. The forward and backward carrier fluxes nearly balance in this region as suggested by Fig. 1 imagined with a constant quasi-Fermi level. When a device is well within the low-mobility limit, the quasi-equilibrium region becomes of primary importance because the potential drop across it determines the carrier density at the edge of the region, while the assumptions necessary for the validity of injection-limited (e.g. Fowler-Nordheim) models no longer hold. In this limit, the flux is determined both by the transport process and the carrier density at the edge of the quasi-equilibrium region.

B. Solving the transport equation

A quantitative description of the carrier profiles and fluxes is obtained from the electronic continuity and transport equations (5) and (6). The presence of the tunneling flux and recombination terms complicates the solution of these equations. Due to recombination, the quantity F_e will not be spatially constant at steady state. The related quantity $F_e^{\text{inj}} \equiv F_e + \zeta_e$, however, is constant at steady state. Physically, F_e^{inj} represents the total number of electrons being injected into the device per unit time. We now define the function θ_e,

$$\theta_e \equiv \frac{F_e - \tau_e}{F_e^{\text{inj}}} = 1 - \frac{\tau_e + \zeta_e}{F_e^{\text{inj}}} \tag{31}$$

because this allows us to write the transport equation (6) in the form $F_e^{\text{inj}}\theta_e = \phi' n_e - n_e'$, whose solution is

$$n_e(x) = e^\phi \left(n_e(0) - F_e^{\text{inj}} \int_0^x \theta_e e^{-\phi}\, dx \right) \tag{32}$$

This is convenient because all of the effects of tunneling and recombination are parameterized via the occurence of θ_e in the integral. The meaning of θ_e can be understood by noting that it is very nearly 1 in any region where neither tunneling or recombination are significant, and is very nearly 0 wherever tunneling is the main contribution to the injected flux or wherever most of the electrons have recombined. Combining Eq. (32) evaluated at $x = L$ with the boundary conditions $n_e(0) = 1 - \lambda_F F_e^{\text{inj}}$ and $n_e(L) = 1 + \lambda_F F_e^{\text{inj}}$ gives

$$F_e^{\text{inj}} = \frac{1 - e^{-V}}{\theta_e(0)\lambda_F + \int_0^L \theta_e e^{-\phi}\, dx + e^{-V-\delta}\theta_e(L)\lambda_F} \tag{33}$$

The numerator of this expression represents the amount of charge that can flow between two electrodes whose potentials differ by V. The denominator represents the "effective resistance" of the device, which is in the form of three series resistances: an injection electrode resistance, an interior or transport resistance, and an ejection electrode resistance. From Eq. (33), one may immediately derive three important limiting behaviors of the system, in which the flux is dominated by the largest resistance. The *injection-limited flux* is $\lambda_F^{-1}(1 - e^{-V}) + \tau_e(0)$ (sum of a thermionic emission and a tunneling injection term), and the *ejection-limited flux* is $e^\delta \lambda_F^{-1}(e^V - 1) + \tau_e(L) + \zeta_e(L)$ (sum of an "ideal diode" term, tunneling ejection term, and an additional term including all the electrons that recombined on their way to the ejection electrode). The *transport-limited flux* is $(1 - e^{-V})[\int_0^L \theta_e e^{-\phi} \, dx]^{-1}$, which cannot be described without detailed knowledge of ϕ and θ_e. However, in low-mobility systems, λ_F will typically be small enough that the flux will be transport limited.

Tunneling plays an important role in determining device behavior because of the electronic quasi-equilibrium it establishes throughout some portion of the device. This manifests itself through the occurrence of θ_e in the resistance integral; specifically, the tunneling process acts to decrease the resistance by causing θ_e to become small throughout a region of the device near the electrode. Low mobilities tend to facilitate the formation of the quasi-equilibrium region by making λ_F small. We obtain the asymptotic ($\lambda_F \to 0$) solution for θ_e in the tunneling region ($0 < x < x_1$) and in the absence of recombination by combining Eqs. (5), (6) and (32) (see Appendix C),

$$\theta_e \sim \exp\left(-\int_x^{x_1} \sqrt{\frac{\phi' \kappa_e}{\lambda_F}} \, dx\right) \tag{34}$$

It is important to have an explicit expression for θ_e in order to be able to describe the charge densities, such as when calculating the quasi-equilibrium condition in section V A. The effective edge of the quasi-equilibrium region established by tunneling, x_τ, is defined as the inflection point of θ_e. Conceptually it is helpful to imagine θ_e as a step function whose step is located at x_τ. By comparing to simulations we have found that this forms a good basis for approximating the integrals, so that e.g. $\int_0^{x_1} \theta_e e^{-\phi} \, dx \approx \int_{x_\tau}^{x_1} e^{-\phi} \, dx$.

V. MIXED IONIC/ELECTRONIC SYSTEM

In this section we analyze the behavior of mixed ionic/electronic systems in the transport-limited regime, corresponding to the low-mobility (small λ_F) limit.

We have seen that the ionic polarization process produces double layers near the electrodes where the potential is rapidly changing along with a wider bulk region in which the potential is nearly constant. Each of these regions contribute to the transport resistance. Because of the very different nature of the double layer and bulk regions, we treat the effective resistances of these regions separately by splitting the integral in Eq. (33) into double layer and bulk contributions,

$$\int_0^L \theta_e e^{-\phi} \, dx = \left(\int_0^{x_-} + \int_{x_-}^{x_+} + \int_{x_+}^L\right) \theta_e e^{-\phi} \, dx \tag{35}$$

In a manner analogous to the limits discussed in the previous section, the transport-limited flux itself will be limited by the largest integral. If one of the double layer integrals is larger than the bulk integral, then the flux is *double-layer limited*. If the bulk integral is larger, the flux is *bulk limited*.

Below we give a method for determining which limit a given system is in. Using this we will establish that low-mobility systems tend to be bulk limited, so we then analyze in detail the behavior of bulk-limited systems. By doing so, we provide a description of the continuum of current-voltage behavior expected for widely studied LECs in which the electronic carrier mobility is generally low.

A. Electronic quasi-equilibrium in the double layers and the criteria for bulk-limited conduction

Electronic injection in LECs[5,6] and related electrochemical systems[42] is frequently treated by assuming that the quasi-Fermi levels are constant (carrier concentrations are at quasi-equilibrium) throughout the double layers, leading to bulk-limited conduction. This assumption is equivalent to using the Nernst equation as a boundary condition. In this section, we present results that can be used to determine the validity of the quasi-equilibrium assumption and hence of bulk-limited conduction; as before, we give results for electrons.

The basis for determining the extent of the quasi-equilibrium region is the injected flux Eq. (33). In the transport-limited regime, $n_e(0) \approx 1$. One can then see from Eq. (32) that $n_e \approx e^\phi$ – i.e., is at quasi-equilibrium – throughout the
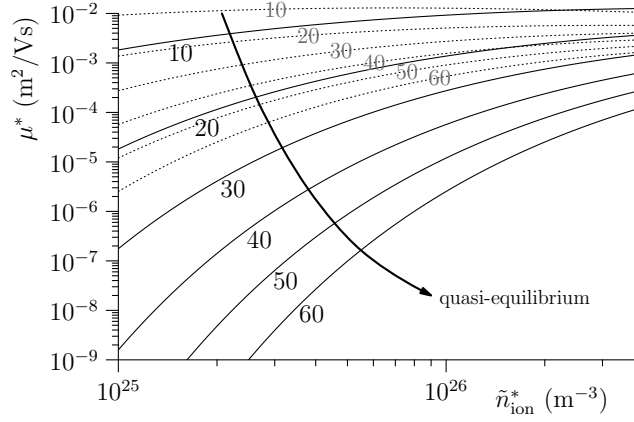
FIG. 5. Approximate double-layer potential drops at which the system begins to deviate from bulk-limited behavior, indicated as curves labeled in thermal volts, as a function of equilibrium ion density and electronic mobility (Eq. (36)). The solid lines are for injection into a one-ion depletion region ($\rho = 1$), and the dotted curves are for injection into a saturation region with $\rho = 10$.

region where the integral $\int_0^x \theta_e e^{-\phi}\, dx$ is much smaller than $1/F_e^{\mathrm{inj}}$; the location at which these quantities approach each other is effectively the edge of the quasi-equilibrium region. Since in the transport-limited regime $1/F_e^{\mathrm{inj}} \approx \int_0^L \theta_e e^{-\phi}\, dx$, this edge can be defined as the point x_{eq} where $\int_0^{x_{\mathrm{eq}}} \theta_e e^{-\phi}\, dx = \int_{x_{\mathrm{eq}}}^L \theta_e e^{-\phi}\, dx$. The electrons will be at quasi-equilibrium throughout the double layer (the *quasi-equilibrium condition*) if $x_{\mathrm{eq}} > x_-$ or equivalently if $\int_0^{x_-} \theta_e e^{-\phi}\, dx < \int_{x_-}^L \theta_e e^{-\phi}\, dx$.

We will evaluate the quasi-equilibrium condition for a quadratic potential in the double layer (as in a fully depleted or saturated layer). Neglecting recombination in the double layer, $\int_0^{x_-} \theta_e e^{-\phi}\, dx \approx \int_{x_\tau}^{x_-} e^{-\phi}\, dx$ (see discussion following Eq. (34)). Assuming large k_e, the carriers will recombine abruptly at a point x_ζ, causing θ_e to approach 0; we therefore approximate θ_e as a step function so that $\int_{x_-}^L \theta_e e^{-\phi}\, dx \approx \int_{x_-}^{x_\zeta} e^{-\phi}\, dx$. Evaluating and comparing these two integrals (see Appendix C) gives the quasi-equilibrium condition

$$\lambda_F < \frac{4 \exp\left[-\sqrt{\rho/8\lambda_\nu^2}\left(w_i\sqrt{w_i^2 - w_\tau^2} - rw_\tau^2\right)\right]}{w_\tau(1/\sqrt{\rho}w_\tau^2 + r/\sqrt{2}\lambda_\nu)^2} \tag{36}$$

where ρ is the absolute value of the excess charge density in the layer, $w_i = \sqrt{2\Delta\phi_-/\rho}$ is the width of the ionic compact region, $w_\tau = \sqrt{2/\rho}\,\mathrm{erfi}^{-1}(w_D\sqrt{2\rho/\pi}) \approx \sqrt{\ln(\rho w_D^2 \ln(\rho w_D^2))/\rho}$, $r = \ln(w_i/w_\tau + \sqrt{(w_i/w_\tau)^2 - 1})$, and $w_D = x_\zeta - x_-$ is the width of the bulk diffusion region.

Fig. 5 is a contour plot of the quasi-equilibrium condition in terms of the ionic density and electronic carrier mobility, indicating the transition into bulk-limited conduction. The contours represent the potential drops across the double layers (not the applied bias); these potential drops generally do not exceed the band gap. This result shows that the presence of a large amount of ions greatly assists in the formation of a quasi-equilibrium region. Even systems that lie outside of the bulk-limited regime on this diagram may not deviate much from quasi-equilibrium behavior; in particular, even larger mobilities are required to reach injection- or ejection-limited regimes such as those found in typical nonionic crystalline semiconductors. This analysis shows that the assumption of quasi-equilibrium throughout the double layers is valid for a wide range of conditions in systems with high ion content and low electronic mobilities, and for this reason we focus on the bulk-limited regime for the remainder of this work.

It is also noted that, within the bulk-limited regime, the precise forms of the potential profiles and carrier distributions within the ionic double layers are not important to the overall device flux, because the flux is only determined by the potential drops across these layers. Indeed, certain treatments essentially neglect the double layers[5,6,42] by taking their edges to be the boundaries of the MIEC and relating the carrier concentrations there to the electrode quasi-Fermi levels by the Nernst equation.[38] When the quasi-equilibrium condition holds, the concentration at the edge of the double layer is $n_e(x_-) = e^{\Delta\phi_-}$.
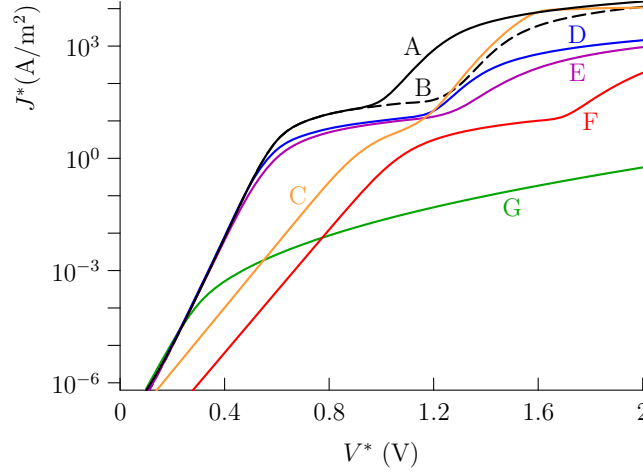
FIG. 6. Current density $J^* = qF^*_{\text{dev}} = q(F^*_e - F^*_h)$ as a function of bias. Curves A and B show one-ion systems (mobile anions) with bulk-limited conduction, with $\mu^*_e = \mu^*_h = 10^{-10}\,\text{m}^2/\text{Vs}$, $\tilde{n}^*_{\text{ion}} = 10^{26}\,\text{m}^{-3}$, $\hat{n}^*_a = 10^{27}\,\text{m}^{-3}$, $\tilde{n}^*_e = 10^{16}\,\text{m}^{-3}$, and $\tilde{n}^*_h = 10^{16}\,\text{m}^{-3}$ (A), $\tilde{n}^*_h = 10^{12}\,\text{m}^{-3}$ (B). Curve C shows a two-ion system with the same parameters as curve B and $\hat{n}^*_c = \hat{n}^*_a$, $\mu^*_h = 2 \cdot 10^{-10}\,\text{m}^2/\text{Vs}$. Curve D shows the same system as in curve B except with $\tilde{n}^*_{\text{ion}} = 10^{25}\,\text{m}^{-3}$, $\hat{n}^*_a = 10^{26}\,\text{m}^{-3}$. Curves E and F illustrate loss of quasi-equilibrium, showing the same system as curve D but with $\mu^*_e = \mu^*_h = 10^{-4}\,\text{m}^2/\text{Vs}$ and $\mu^*_e = \mu^*_h = 1\,\text{m}^2/\text{Vs}$, respectively; curves E and F are scaled down by the ratios of their mobilities to that of curve D. Curve G shows the system from curve A with $\tilde{n}^*_{\text{ion}} = 10^{23}\,\text{m}^{-3}$.

B. Regimes of operation with bulk-limited conduction

In this section, we synthesize all of the previous results to obtain quantitative descriptions of bulk-limited MIEC systems. We restrict the analysis in this section to $\delta = 0$ because systems with nonzero δ introduce additional complications that are beyond the scope of this work to address.

Figure 6 shows simulations of current density (J^*)-voltage curves for a variety of systems, illustrating both bulk-limited conduction and deviation from it as the quasi-equilibrium condition becomes violated. Curves A, B and D are results for bulk-limited one-ion systems showing how they change with $\tilde{n}^*_e$, $\tilde{n}^*_h$, and $\tilde{n}^*_{\text{ion}}$. Curve C shows a bulk-limited two-ion system, which has a similar shape to the one-ion systems. Experimental curves similar in shape to the the bulk-limited curves of Fig. 6 have been reported in the literature.[6,43–46] The simulations also show that changing μ^*_e and μ^*_h while leaving their ratio unchanged (provided they do not become too large) only alters the magnitude of J^* and not the shape of the current-voltage curve. At sufficiently high mobilities, however, transport will no longer be bulk limited. For instance, the contour plot of Fig 5 and Eq. (25) predict the loss of quasi-equilibrium at $V^* \approx 0.5$ V for the relatively high-mobility system of curve E ($\tilde{n}^*_{\text{ion}} = 10^{25}$ and $\mu^* = 10^{-4}\,\text{m}^2/\text{V s}$), and indeed this curve begins to deviate from the lower mobility, bulk-limited system (Curve D) at this voltage. The mobilities required to observe the loss of quasi-equilibrium at reasonable ion loadings are much larger than those found in typical LEC systems (approaching those of crystalline inorganic semiconductors). The mobilities and ion loadings found in typical LEC systems place them in the quasi-equilibrium regime. Note that quasi-equilibrium is lost even for low-mobility systems when the ion concentration is sufficiently low (curve G).

For the remainder of this section, we specifically investigate bulk-limited conduction by assuming that the quasi-equilibrium condition holds. We focus on the results for large k_s because of our emphasis on low-mobility systems. We also assume that the width of the bulk region is much larger than that of the double layers.

There are four clearly distinguishable regimes of behavior. In Fig. 7, we show a representative current density-voltage curve obtained from simulations, in which each of these regimes can be observed. Fig. 7 also shows the recombination current, which is approximately proportional to the light output of an LEC (neglecting for instance quenching by the electrodes).

Below we will provide approximate expressions for the biases at which a given system transitions between each regime and the device fluxes in each regime. Fig. 7 compares the expressions for the transition voltages (V_1, V_2, and V_3) and device fluxes (solid lines) to full numerical simulations of a representative one-ion system. We will also provide simulation data depicting the charge densities and electrostatic potential to provide a physical picture of the underlying mechanisms. The device fluxes are given in physical units, and the device flux is defined as $F^*_{\text{dev}} \equiv F^*_e - F^*_h$, as this is the physically measurable flux.
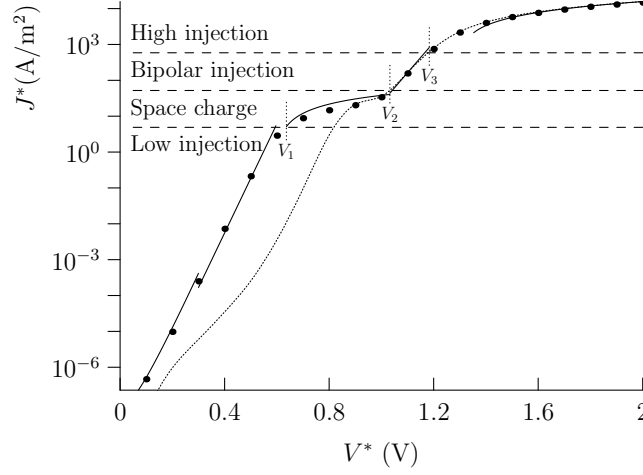
FIG. 7. Comparison of simulated current density (dots) to analytical approximations (lines) for a one-ion system with mobile anions, $\tilde{n}_{\text{ion}}^* = 10^{26}\,\text{m}^{-3}$, $\hat{n}_a^* = 10^{27}\,\text{m}^{-3}$, $\tilde{n}_e^* = \tilde{n}_h^* = 10^{16}\,\text{m}^{-3}$, and $\mu_e^* = \mu_h^* = 10^{-10}\,\text{m}^2/\text{Vs}$, showing each regime and the transition biases. The low injection regime uses Eq (37) combined with (27) for $V^* < 0.3$ (pre-saturation) and (25) for $V^* > 0.3$ (post-saturation). The remaining regimes use Eqs. (39), (41), and (43). In the high injection regime, Eq. (43) does not become valid until the ions have completely polarized, at a bias slightly beyond V_3^*. The dotted line shows the simulated total recombination current (proportional to light output). Note that it is orders of magnitude below the device current until the system approaches the bipolar injection regime, after which it follows the device current.

1. The low-injection limit

In the low-injection limit, there are not enough electronic carriers to affect the potential profile, so ϕ is determined entirely by the ions; we can therefore use the results of Sec. III to determine the potential drops and to justify the field-free bulk assumption. Because the bulk is field-free, the electronic carriers simply diffuse through the bulk and have a linear profile. A typical example of a system in this regime is shown in Fig. 8.

The following approximation holds independently of recombination (Appendix D 1):

$$F_{\text{dev}}^* \approx \frac{D_e^* \tilde{n}_e^* e^{q\Delta\phi_-^*/kT}}{L^*} + \frac{D_h^* \tilde{n}_h^* e^{q\Delta\phi_+^*/kT}}{L^*} \tag{37}$$

Such diffusion flux expressions have been presented by a number of authors investigating MIECs with field-free bulk regions;[4,47,48] indeed, deMello et al. give essentially the same result in terms of carrier concentrations at the double layer edge.[4] By combining Eq. (37) with the results of section III for $\Delta\phi_-^*$ and $\Delta\phi_+^*$, one can obtain the flux explicitly in terms of the applied bias.
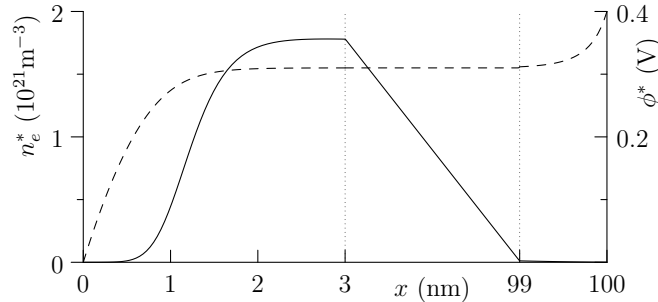

FIG. 8. Low-injection regime in the one-ion system from Fig. 7 at $V^* = 0.4\,\text{V}$, showing the electron density profile (solid line) and electrostatic potential profile (dashed line). The electrons rise rapidly from their electrode value $\tilde{n}_e^*$ to their value at the double layer edge as determined by quasi-equilibrium, $\tilde{n}_e^* e^{q\Delta\phi_-^*/kT}$. They then diffuse through the field-free bulk with a characteristic linear profile.

Because charge injection is in general asymmetric, the recombination zone will be near the electrode where the minority carriers are injected. In this regime, the total recombination current (and hence light output) is proportional to the injected minority carriers, which will in general not be proportional to the device flux, as illustrated in Fig. 7.

2. "Space-charge-limited" injection

The mechanism of device behavior in this regime is similar to that of space charge effects in semiconductors, but it is distinct from the classical space-charge-limited conduction model.[49] At the onset of the space-charge-limited regime, the injected majority charges begin to affect ϕ in such a way that retards their further injection, the flux then increasing very slowly with V (see Fig. 7). The transition into this regime occurs when the majority carrier concentration reaches a certain proportion of the ionic concentration.

In most systems there will be a high enough degree of asymmetry that one of the carriers will dominate in the low-injection regime. In one-ion systems, the potential drop across the depletion double layer is generally so much larger than that across the accumulation layer (see Fig. 25) that the carrier injected at the depletion side will tend to dominate. For example, with mobile anions, if $\tilde{n}_h < \tilde{n}_e$, the electron concentration will overtake the hole concentration near the bias $V \approx \hat{n}_a/(\hat{n}_a - 2) \ln(\tilde{n}_h/\tilde{n}_e)$; as long as the transition into the space-charge-limited regime occurs above this bias, we can assume that injection at the depletion side dominates. With two-ion systems, the crossover in dominant carrier occurs at the bias $\hat{n}_a\hat{n}_c/(\hat{n}_c - \hat{n}_a) \ln(\tilde{n}_h/\tilde{n}_e)$. In the special case of $\hat{n}_a = \hat{n}_c$ and $\tilde{n}_e = \tilde{n}_h$, this regime will not occur because the two electronic species are present in equal proportions.
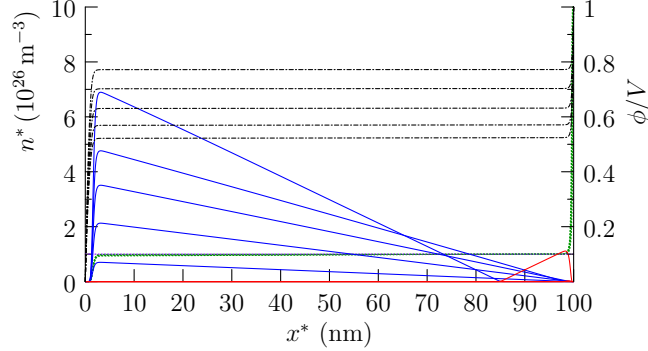

FIG. 9. The space-charge-limited regime for the same system as in Fig. 7, from $V^* = 0.6\,\mathrm{V}$ to $1.0\,\mathrm{V}$ in $0.1\,\mathrm{V}$ intervals. The electron (blue) and hole (red) distributions have been multiplied by 100 for comparison with the anions (green, dashed) and fixed cations (purple, dashed). Note the relatively slow (approximately linear) increase of the majority carriers, and the appearance of the minority carriers near the upper end of this regime. The electrostatic potential ϕ normalized by V is also shown (dash-dotted lines); the applied bias functions mainly to increase the potential drop at the hole-injecting side (right) until the drops are approximately equal, signaling the onset of the bipolar injection regime.

A one-ion system in the space-charge-limited regime is depicted in Fig. 9. When the majority carrier's concentration reaches the magnitude at which space-charge effects become significant, the potential drop at the side where it is injected will suddenly begin to increase very slowly with V. This causes the majority carrier concentration to increase much less rapidly than the exponential increase observed in the low-injection regime, and because the extra potential provided by any additional bias then is dropped mainly at the minority carrier-injecting electrode, it causes the minority carrier to be injected much more rapidly. Such a shift from predominately increasing the injection rate of one carrier to that of the other has been noted by deMello et al. as well.[4] The transition into the space-charge-limited regime is characterized by a sudden transition to a much weaker V dependence of the electronic flux (see Fig. 7). By expanding the potential drops to first order in the total excess charge $\int_0^L n_h - n_e \, dx = \phi'_L - \phi'_0$, we obtain a simple approximation to the bias at which this transition occurs (Appendix D 2):

$$V_1^* \approx \frac{kT}{q} \left[A_{\hat{n}} \ln \left(\frac{\lambda}{L^*} \frac{B_{\hat{n}} \tilde{n}_{\mathrm{ion}}^*}{\tilde{n}_{\mathrm{maj}}^*} \right) + C_{\hat{n}} \right] \tag{38}$$

where $\tilde{n}_{\mathrm{maj}}^*$ is the equilibrium value of the majority carrier. For one-ion systems, $A_{\hat{n}} = \hat{n}/(\hat{n} - 1)$, $B_{\hat{n}} = 2\hat{n}(\hat{n} - 1)$ (saturation limit) or $B_{\hat{n}} = 2 \ln^2(\lambda/L^*\tilde{n}_{\mathrm{ion}}^*)$ (diffuse limit), and $C_{\hat{n}} = 0$; for two-ion systems, $A_{\hat{n}} = (\hat{n}_a + \hat{n}_c)/\hat{n}_{\mathrm{maj}}$,
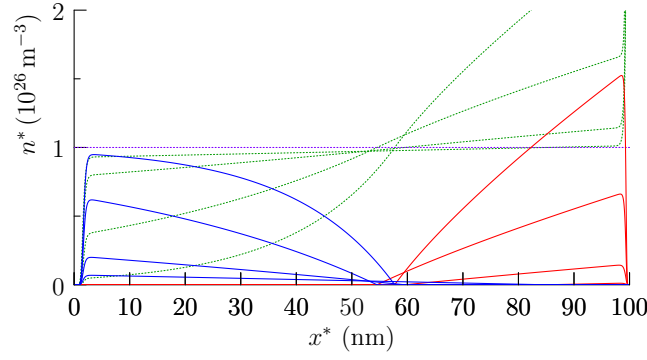
FIG. 10. The bipolar injection regime for the same system as in Fig. 7, from $V^* = 1.0\,\mathrm{V}$ to $1.4\,\mathrm{V}$ in $0.1\,\mathrm{V}$ intervals. The electron (blue) and hole (red) distributions have been multiplied by 100 for comparison with the anion (green, dashed) and fixed cation (purple, dashed) distributions. The electron and hole populations are now approximately equal.

$B_{\hat{n}} = 2(\hat{n}_a + \hat{n}_c)/\sqrt{\hat{n}_{\min}}$, and $C_{\hat{n}} = \ln(\hat{n}_{\mathrm{maj}} - 1) - (\hat{n}_{\min}/\hat{n}_{\mathrm{maj}})\ln(\hat{n}_{\min} - 1)$ where $\hat{n}_{\mathrm{maj}}$ and $\hat{n}_{\min}$ are the value of $\hat{n}$ for the same sign of ion as the majority and minority carriers, respectively. This bias brings the majority carrier concentration up to approximately $\hat{n}/L$ (one ion) or $(\hat{n}_a + \hat{n}_c)/\sqrt{\hat{n}_{\min}}L$ (two ions).

In the space-charge-limited regime, the bulk field remains relatively small, and the flux is still mainly due to diffusion of the majority carrier across the bulk. An approximation to the flux is (Appendix D 3)

$$F_{\mathrm{dev}}^* \approx \frac{D_{\mathrm{maj}}^*}{L^{*2}} \sqrt{C_{\hat{n}} \varepsilon \varepsilon_0 \tilde{n}_{\mathrm{ion}}^*/q} \frac{\Delta V^*}{\sqrt{V^*}} \tag{39}$$

where $\Delta V^* = V^* - V_1^* + (A_{\hat{n}} kT/2q)\ln(qV^*/A_{\hat{n}} kT)$, D_{maj}^* is the diffusion coefficient for the majority electronic carrier, $A_{\hat{n}}$ is as defined above, and $C_{\hat{n}} = 2\hat{n}(\hat{n} - 1)$ for one ion, $C_{\hat{n}} = 2\hat{n}_{\mathrm{maj}}(\hat{n}_{\mathrm{maj}}/\hat{n}_{\min} + 1)$ for two ions.

Because the flux is still dominated by the majority carrier, the total recombination rate - and hence the device light output - will depend on the number of injected minority carriers, since in general all of them will recombine with the majority carriers within a short distance from the minority carrier-injecting electrode. The recombination zone will be observed near the contact injecting the minority carriers, and the light output will increase more rapidly than the device flux (see Fig. 7).

3. Bipolar injection

In the space-charge-limited regime, the minority charge concentration builds up rapidly. At a certain bias, the concentrations of electrons and holes approach each other, and the injected electron and hole fluxes become equal because essentially all injected charges recombine in the bulk. This marks the beginning of the bipolar injection regime.

Figure 10 shows the carrier and ion profiles in the bipolar injection regime. Because there are now roughly equal proportions of electrons and holes, the space-charge effects act on the injection of both carriers to an equal extent, effectively cancelling out these effects. This allows both carriers to rise at equal rates, and most of any additional potential applied in this regime is split evenly between the two double layers (the bulk field is still relatively small). This results in a sudden increase of the device flux, as what was previously the majority carrier can now be injected more rapidly than in the space-charge-limited regime. The recombination and light output will now follow the device flux (see Fig. 7), and the recombination zone will be closer to the electrode injecting the carrier with the smaller mobility.

A simple calculation (Appendix D 4) shows that the densities of holes and electrons approach each other, and therefore the second transition occurs, near the bias

$$V_2^* \approx \frac{kT}{q} \ln\left(\sqrt{\frac{\mu_{\mathrm{maj}}^*}{\mu_{\min}^*}} \frac{\lambda^2}{L^{*2}} \frac{C_{\hat{n}} \tilde{n}_{\mathrm{ion}}^{*2}}{\tilde{n}_e^* \tilde{n}_h^*}\right) \tag{40}$$

where $C_{\hat{n}} = 4\hat{n}^2$ (saturated limit) or $C_{\hat{n}} = 4\ln^4(\lambda/L^*\tilde{n}_{\mathrm{ion}}^*)$ (if the system is in the diffuse limit at V_1) for one ion, and

$C_{\hat{n}} = 4(\hat{n}_a + \hat{n}_c)^2/\hat{n}_{\min}$ for two. In this regime the flux is (Appendix D 5)

$$F_{\mathrm{dev}}^* \approx \frac{D_{\mathrm{eff}}^* \tilde{n}_{\mathrm{eff}}^*}{L^*} \exp\left(\frac{qV^*}{2kT}\right) \tag{41}$$

where $\tilde{n}_{\mathrm{eff}}^* = \sqrt{\tilde{n}_e^* \tilde{n}_h^*}$ and $D_{\mathrm{eff}}^* = \sqrt{D_e^* D_h^*}((D_e^*/D_h^*)^{1/4} + (D_h^*/D_e^*)^{1/4})$. The dependence of V_2^* on $\tilde{n}_e$ and $\tilde{n}_h$ is clearly illustrated by comparing curves A and B of Fig. 6.

4. High injection

As the magnitude of the injected charge continues to increase, the ions will be increasingly displaced from the bulk in order to maintain electroneutrality. Eventually the electronic concentrations will reach the ionic concentrations, marking the onset of the high-injection regime.

Figures 11 and 12 show the carrier and electrostatic potential profiles in the high-injection regime in one- and two-ion systems. In this regime most of the additional applied potential beyond the transition bias will develop across the bulk region; the nature of this region is the primary difference between one- and two-ion systems in the high-injection regime. The bias at which the transition into the high-injection regime begins to occur is the minimum required to bring the electronic carrier concentrations up to the ionic concentration,

$$V_3^* \approx \frac{E_G^*}{q} - \frac{kT}{q} \ln \frac{N_C N_V}{\tilde{n}_{\mathrm{ion}}^{*2}} \tag{42}$$

where E_G^* is the bandgap and N_C, N_V are the effective density of states constants in the bands.

Smith has addressed the two-ion high-injection regime,[2] obtaining the same transition bias. However, his work includes an ion association/dissociation mechanism absent from ours. With such a mechanism, when the free ion concentration is relatively low, the associated salt molecules form a "reservoir" that acts to prevent the junction region from being depleted of ions, in turn leading to a stronger dependence of the flux on the applied bias. At biases greater than V_3^*, however, these salt molecules will soon become depleted, and the system will behave as though the pairing mechanism is not present.

There are a number of similarities between one- and two-ion systems in the high-injection regime. In both cases, the device consists essentially of five distinct spatial regions, from left to right: (1) the cathode double layer, (2) a neutral region containing electrons and cations, (3) a narrow region in which most of the recombination occurs, (4) a neutral region containing holes and anions, and (5) the anode double layer.

After reaching V_3^*, the ions will begin to separate completely and move toward the neutral regions until each electronic carrier is completely compensated by ions of the opposite charge. This compensation is apparent from comparing the ionic and electronic carrier profiles in Figs. 11 and 12. Note that in the one-ion system of Fig. 11, the mobile anions compensate both the injected holes and immobile cations on the anode side of the device. The complete separation of ions requires a small amount of additional potential ξV_T beyond V_3^*, as much of this potential is dropped across the bulk. Therefore, in the flux expressions that follow, we define $\Delta V^* = V^* - V_3^* - \xi V_T$. Numerical simulation suggested estimates of $\xi \approx 6$ for one-ion systems and $\xi \approx 10$ for two-ion systems. When $\Delta V^* > 0$, the ions have completely polarized, and the concentrations at the edges of the neutral regions increase slowly with bias. Unless $\hat{n}$ is small, these concentrations generally will not reach $\hat{n}$ under normal operating conditions. In the following analysis, we have assumed that this is the case; hence, the device fluxes in this regime are independent of $\hat{n}$. As before, the recombination current follows the device flux in the high-injection regime (see Fig. 7).

In two-ion systems, the voltage V_3^* essentially represents the transition between the applicability of the so-called electrodynamic model,[29] in which the bulk field is negligible, and the electrochemical model,[1] in which the bulk contains a junction region depleted of ions and is characterized by a large field. Equation (42) was derived assuming bulk-limited transport. If electrode limitations are present, the injected carrier concentration will be reduced, and the transition into the high-injection regime will shift to higher voltages. Reenen and coworkers have conducted simulations and experiments addressing this point, again illustrating the continuum of behavior between the electrodynamic and electrochemical models.[19] Electrode limitations act to destroy quasi-equilibrium in a manner similar to lowering the ion content or increasing the electronic carrier mobility of the MIEC, as evidenced by comparing curves F and G in Fig. 6 to curves D and A.

a. One-ion systems. In this case the majority of any additional applied potential is dropped across the neutral region containing only the immobile ions, where the field and carrier profiles are approximately constant (see Fig. 11), and the flux is almost entirely due to drift. The carrier concentration on the other side, where the carriers are compensated by the mobile ions, will increase slowly with bias; this carrier's flux is driven by both drift and
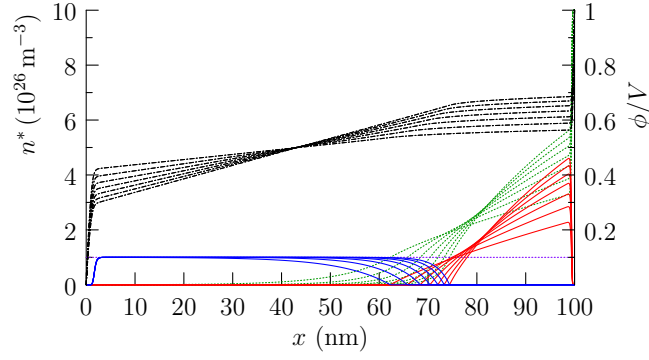
FIG. 11. One-ion high-injection regime for the same system as in Fig. 7, showing electron/hole profiles (blue/red solid lines), anion/cation profiles (green/purple dotted lines), and electrostatic potential profile (dash-dotted) normalized by the applied voltage, for $V^* = 1.4$ V to 2.0 V in increments of 0.1 V. The applied potential now drops increasingly across the neutral region depleted of mobile ions.
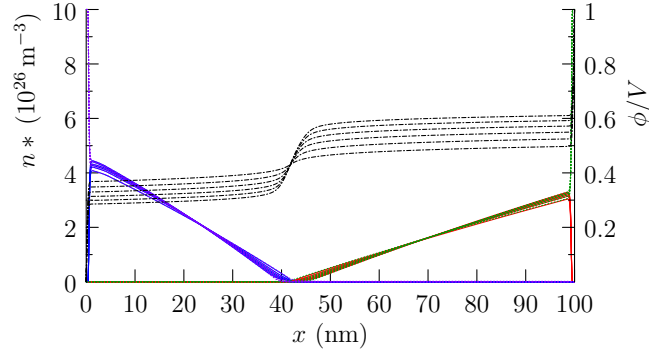

FIG. 12. Two-ion high-injection regime for the two-ion system from Fig. 6 (curve C), showing electron/hole profiles (blue/red solid lines), anion/cation profiles (green/purple dotted lines), and electrostatic potential profile (dash-dotted) normalized by the applied voltage, for $V^* = 1.7$ V to 2.2 V in increments of 0.1 V. Note the steady increase in the junction potential drop and the very slow increase of the concentrations and the junction width. The recombination zone is closer to the electrode injecting the carrier with the smaller mobility (near $L^*/(1 + \sqrt{\mu_h^*/\mu_e^*}) \approx 41$ nm). The potential drop across the anode double-layer is larger because of the holes' smaller electrode concentration ($\tilde{n}_h/\tilde{n}_e = 10^{-4}$).

diffusion throughout the neutral region. The recombination zone will move closer to the electrode that injects carriers compensated by mobile ions as the bias is increased. The device flux in this regime is approximately (Appendix D 6 a)

$$F_{\text{dev}}^* \approx \frac{\tilde{n}_{\text{ion}}^*}{L^*} \left(2D_2^* + \mu_1^* \Delta V^* + 2\sqrt{D_2^{*2} + D_2^* \mu_1^* \Delta V^*} \right) \tag{43}$$

where μ_1^* is the mobility of the carrier with the same sign of charge as the mobile ions and D_2^* is the diffusion coefficient of the carrier with that of the immobile ions.

b. *Two-ion systems.* The main characteristic of two-ion systems in this regime is the formation of a "junction" in the bulk of the device, depleted of ions and possessing a relatively large field, where most of the recombination occurs. Previous work has described the properties of this kind of junction.[2,5]

The junction forms when the device flux reaches approximately $4\tilde{n}_{\text{ion}}^*(\sqrt{D_e^*} + \sqrt{D_h^*})^2/L^*$, and its location is approximately $L^*/(1 + \sqrt{D_h^*/D_e^*})$. After the junction is fully formed, most of the additional applied bias will drop across the junction (see Fig. 12), as has been observed in certain experimental systems.[17,19] A small amount of the bias will act to increase the concentrations at the double-layer edges, which increase very slowly with bias; the near constancy of these concentrations has been observed experimentally.[50] Transport through the neutral regions occurs via both drift and diffusion.

Solving for the flux using approximations similar to those that led to Eq. (43) requires the solution of a third order

polynomial (Appendix D 6 b). Here we give a first-order Padé approximant of that solution,

$$F_{\text{dev}}^* \approx \frac{4 A_D \tilde{n}_{\text{ion}}^*}{L^*} \frac{1 + 1.529 (\Delta V^* \lambda / V_T L^* B_D)^{2/3}}{1 - 1.092 (\Delta V^* \lambda / V_T L^* B_D)^{2/3}} \tag{44}$$

where $A_D = (\sqrt{D_e^*} + \sqrt{D_h^*})^2$ and $B_D = 2 + \sqrt{D_e^*/D_h^*} + \sqrt{D_h^*/D_e^*}$.

VI. SUMMARY

Our analysis of MIECs is based on an ionic model characterized by a modified drift-diffusion transport equation that explicitly accounts for volume constraints, and an electronic model distinguished by the inclusion of a spatially dependent tunneling process that accounts for both forward and backward fluxes, as well as the quasi-equilibrium that occurs in low-mobility materials. By combining these models and examining their interactions, we have delineated the major regimes of operation of an idealized MIEC with high ion content and low electronic mobilities, and provided analytical results consistent with simulations of the basic equations.

The modified ionic transport equation reveals several unique properties and differences between one- and two-ion systems. Both systems display depletion and accumulation layers near the electrodes which grow into the device as the bias is increased. In one-ion systems, these layers may meet each other, in which case the ions will no longer be able to screen the electrode fields. In two-ion systems, the bulk may become depleted of ions, leading to a loss of field screening; two-ion systems have less of an ability to screen the electrode fields than one-ion systems do. Furthermore, the relative values of the double layer potential drops in these systems are different because of the different amounts of charge that can build up in the ionic double layers. This leads to differing dependencies of the electronic current on bias, especially at small voltages where there is a relatively low level of electronic charge injection.

The electronic injection model incorporates both thermal emission and tunneling, and tunneling is treated in a spatially-dependent manner. There are two important consequences of this kind of model: (1) if the electronic mobilities are large, then the injected carrier concentrations may become very small near their injecting electrode, leading to reverse-biased Schottky contact and Fowler-Nordheim-type flux expressions; (2) if the electronic mobilities are small, the injected carriers reach quasi-equilibrium throughout some region extending from the electrode, making Fowler-Nordheim-type expressions invalid and favoring the applicability of the Nernst equation.

The substantial increase in electronic current caused by the polarization of ions in MIECs has long been recognized. We have shown, in low-mobility systems, that this increase is not, as is often posited, simply due to increased tunneling injection caused by the narrowing of the potential profiles near the electrodes. Instead, it is due to the fact that these narrowed profiles can allow the electrodes to reach quasi-equilibrium with the electronic carriers at the inner edges of the double layers - the low mobilities of these carriers actually cause the tunneling injection and ejection (backflow) currents to be nearly equal, allowing quasi-equilibrium to occur. The high rate of tunneling transfer, while responsible for the large exchange current that leads to quasi-equilibrium, does not determine the device current. This may seem like somewhat of a subtle distinction in mechanism, but it does lead to a very different functional form for the current; indeed, it shows that in a low-mobility system, applying the Nernst equation across the double layers is much more appropriate than applying a model such as Fowler-Nordheim near the electrode. Eq. (36) provides a means by which to estimate the presence of quasi-equilibrium in a given system. We reiterate that this condition applies only to our idealized model, and there will inevitably be additional considerations in a real physical system, such as imperfect electrodes, material disorder, additional injection barriers, impairment of ion mobility, image-charge effects, etc. Regardless, the central idea remains that fast injection kinetics (relative to the rate of transport) mainly influence the device current through the establishment of quasi-equilibrium.

Assuming that quasi-equilibrium holds across the double layers, we have analyzed systems with bulk-limited conduction, separating the device behavior into four distinct regimes.

In the first regime, there are small amounts of injected charge, small enough so that the electrostatic potential is determined almost entirely by the ions. In this regime, current rises exponentially with bias and the bulk remains field-free, leading to purely diffusive transport. Recombination, and thus light output, does not generally follow the device flux unless the electrons and holes are injected in roughly equal proportions.

The second regime occurs when the majority carrier concentration becomes sufficiently large that it begins to affect the electrostatic potential. This causes any further applied bias to be dropped across the double layer near the electrode where the minority carrier is injected, causing a rapid increase in the minority carrier concentration. In this regime, the total device flux increases slowly with increasing bias, and light output is proportional to the injected minority carrier concentration, which is at most $\propto e^V$. The bias range over which this regime occurs depends on the imbalance of the majority and minority carrier injection.

The third regime occurs when the increased minority carrier injection causes the minority carrier concentration to approach that of the majority carrier. In this regime, both carriers increase relatively rapidly and at approximately

the same rate. Light output is proportional to the device flux in this regime. This regime is fairly narrow however because both carriers increase approximately as $\propto e^{V/2}$.

The fourth regime occurs when the electronic carrier densities approach the ionic densities. A significant bulk field begins to develop. In one-ion systems, the electronic carriers meet and recombine near the edge of the ionic accumulation region. In two-ion systems, they meet somewhere in the bulk, forming a "junction" in which there is a large field; the location of this region is determined by the relative values of the electronic mobilities. In this regime the light output also follows the device flux, which increases much more slowly with bias than in the previous regimes.

The drift-diffusion/Poisson model of MIECs exhibits a wide range of behavior. The various models that have been proposed for MIECs appear to lie on a continuum of behavior. Which limiting case is appropriate depends on the chemical makeup of the MIEC and the applied bias, as we have quantified for an idealized model. Though many factors may affect the physical functioning of various devices and may cause significant quantitative deviation from the idealized model, we expect the essential concepts and mechanisms responsible for the different regimes of device behavior to remain valid.

VII.   ACKNOWLEDGEMENT

Appendix A: Ionic Subsystem

In this section, we define the reference point of the electrostatic potential to be $\phi_B = 0$ for mathematical convenience.

1.   Ionic flux equation

The ionic flux equation is derived from the continuous limit of a discrete random walk model in the same way that the standard drift-diffusion equation can be. The device is discretized into cubic cells of width Δx, taken to be the effective ionic diameter. The cells are then grouped into planes parallel to the electrodes, so that there are $L/\Delta x$ planes. In the ith plane there are N_i ions. The ions move with an average drift velocity of zE_i - where z is the ionic species' charge (± 1) and E_i is proportional to the electric field in plane i - and an average thermal velocity of $\pm H$ with equal probability in either direction.

In a small increment of time Δt, the average number of ions attempting to pass from plane i to plane $i+1$ is $N^{\dagger}_{i\rightarrow i+1} = (\Delta t/\Delta x)N_i(\delta_i^+ zE_i + H/2)$, where $\delta_i^+ = 1$ if $zE_i > 0$ and $\delta_i^+ = 0$ otherwise. However, some of these ions may be blocked by ions occupying cells in slice $i+1$. Assuming that the ions are randomly distributed in each slice, the probability that an ion will be blocked is $N_{i+1}/\hat{N}$. The actual number of ions that pass from plane i to plane $i+1$, $N_{i\rightarrow i+1}$, is then the number of ions attempting to pass multiplied by the probability that they are not blocked, i.e. $N_{i\rightarrow i+1} = (1 - N_{i+1}/\hat{N})N^{\dagger}_{i\rightarrow i+1}$. Similarly, the number of ions passing from plane $i+1$ to plane i is $N_{i\leftarrow i+1} = (\Delta t/\Delta x)(1 - N_i/\hat{N})(\delta_{i+1}^- zE_{i+1} + H/2)$, where $\delta_{i+1}^- = 1$ if $zE_{i+1} < 0$ and $\delta_{i+1}^- = 0$ otherwise.

From these results the discrete analogue of the flux is obtained, $(N_{i\rightarrow i+1} - N_{i\leftarrow i+1})/\Delta t$. Allowing Δx and Δt to become infinitesimal gives the flux equation

$$F = zEn(1 - n/\hat{n}) - (H\Delta x/2)n' \tag{A1}$$

which, by comparison to the derivation of the drift-diffusion equation, shows that $E_i = \mu\phi_i'$ and $H = 2D/\Delta x$. These substitutions give the ionic flux equation, Eq. (4).

2.   Integration of Poisson's equation for the ionic subsystem

Poisson's equation for the ionic subsystem is $\phi'' = n_a - n_c$. Because the ionic fluxes are zero at steady state, the steady-state ionic distributions explicitly depend only on ϕ (see Eq. (13)). This permits the use of the identity $f'' = (1/2)(d/df)(df/dx)^2$, which allows one to relate the values of ϕ and ϕ' at two different points,

$$\frac{1}{2}\left(\phi_1'^2 - \phi_2'^2\right) = \int_{\phi_1}^{\phi_2} n_a(\phi) - n_c(\phi)\,d\phi \tag{A2}$$

Using Eq. (13), this integral from 0 to ϕ is

$$\hat{n} \ln \left(1 + \frac{e^{-z\phi} - 1}{\hat{n}} \right) + z\phi \tag{A3}$$

$$\hat{n}_a \ln \left(1 + \frac{e^{\phi} - 1}{\hat{n}_a / n_B} \right) + \hat{n}_c \ln \left(1 + \frac{e^{-\phi} - 1}{\hat{n}_c / n_B} \right) \tag{A4}$$

for one- and two-ion systems, respectively.

3. Field screening

Eq. (A2) with $\phi_1 = 0$ and $\phi_2 = \phi$ is integrated using separation of variables to get Eq. (14). For one-ion systems, considering e.g. anions to be mobile, the integrand of Eq. (14) is approximated as $1/\sqrt{-\phi + \hat{n} \ln \bar{n}}$ as $\phi \to -\infty$, in the depletion region. The effective edge of the depletion region is defined as the point where $\phi = \phi_- \equiv \hat{n} \ln \bar{n}$, which is the edge of the region where this approximation is defined. As $\phi \to \infty$, in the saturation region the integrand is approximated as $1/\sqrt{(\hat{n} - 1)\phi - \hat{n} \ln \hat{n}}$, and the edge of the region is defined as the point where $\phi = \phi_+ \equiv \bar{n}^{-1} \ln \hat{n}$. Both of these approximations are greater than the integrand. Integrating them, substituting $\phi(L) = \phi(0) + V$ and maximizing the resultant expression for $\phi(0)$ gives $w_{\rm cp}$ (Eq. (16)). In the inner region, the argument of the square root is expanded to yield the approximation $1/\sqrt{\bar{n}\phi^2 + \phi_B'^2}$; this is not always greater than the integrand but can be made so by adding $1/6$ on the negative side of the integral and 0.0384 on the positive side. The integral from ϕ_- to ϕ_+ is then bounded by

$$\frac{1}{\sqrt{\bar{n}}} \left[\operatorname{asinh} \left(\frac{\sqrt{\bar{n}}|\phi_-|}{\phi_B'} \right) + \operatorname{asinh} \left(\frac{\sqrt{\bar{n}}\phi_+}{\phi_B'} \right) \right] + \xi \tag{A5}$$

where $\xi = |\phi_-|/6 + 0.0384\phi_+$ and the first expression represents $w_{\rm df} + w_{\rm bulk}$, where $w_{\rm bulk}$ is the width of the bulk region. There is no unique way to split this into diffuse and bulk terms - it is necessary only to ensure that the singularity at $\phi_B' = 0$ is contained in the bulk term. The final result will be the same regardless of this choice; mathematically it is most natural to define $w_{\rm df} = \bar{n}^{-1/2}(\ln(2|\phi_-|) + \ln(2\phi_+))$. In the diffuse limit there will be no accumulation layer contribution to $w_{\rm cp}$, which is then trivially bounded by using $-\phi_0 < V$. The diffuse width is then bounded by numeric integration of the diffuse regions, taking the upper limit in the accumulation region to ∞. Summing these evaluations gives $w_{\rm df} < 3.76$.

We have established the bound $L < w_{\rm cp} + w_{\rm df} + w_{\rm bulk} + \xi$. Defining $f(\phi_B'/\sqrt{\bar{n}}) = \sqrt{\bar{n}}(w_{\rm df} + w_{\rm bulk})$, we then have $\phi_B'/\sqrt{\bar{n}} < f^{-1}(\sqrt{\bar{n}}(L - w_{\rm cp} - \xi))$. The function f can be explicitly inverted,

$$f^{-1}(v) = 2e^{v/2} \frac{\sqrt{(|\phi_-| + \phi_+ e^v)(\phi_+ + |\phi_-|e^v)}}{e^{2v} - 1} \tag{A6}$$

and is then bounded by adding expansions about $v = \infty$ and $v = 0$,

$$f^{-1}(v) < e^{-v/2} \left(2\sqrt{|\phi_-|\phi_+} + \frac{|\phi_-| + \phi_+}{v} \right) \tag{A7}$$

Because $2\sqrt{|\phi_-|\phi_+} = e^{(\sqrt{\bar{n}}/2)w_{\rm df}}$, it is absorbed into the exponent to yield

$$\phi_B' < e^{-\frac{1}{2}\sqrt{\bar{n}}(L - w_{\rm cp} - w_{\rm df} - \xi)} \left(\sqrt{\bar{n}} + \frac{A}{L - w_{\rm cp} - \xi} \right) \tag{A8}$$

where $A = (|\phi_-| + \phi_+)/(2\sqrt{|\phi_-|\phi_+})$. For $\hat{n} < 10^6$, $A < 2$, which gives the one-ion result (Eq. (15)). The two-ion result is derived using the same methods, with $\xi = 0.0201(|\phi_-| + \phi_+)$, which is trivially bounded by $0.0201V < V/49$. In this case $A = 1$ when $\hat{n}_a = \hat{n}_c$ and only deviates much when the two are very different; even at the extreme of e.g. $\hat{n}_a = 10^6$ and $\hat{n}_c = 2.7$ we have $A < 2$.

4. Two-ion saturation before screening

To simplify the calculations we let $\hat{n} \to \infty$. In this case Poisson's equation is $\phi'' = n_B(e^\phi - e^{-\phi})$. Using $\phi(0) = -V/2$, the solution on the cathode side is

$$\phi = -4 \operatorname{atanh}\left(\tanh(V/8)e^{-\sqrt{2n_B}x}\right) \tag{A9}$$

The solution on the anode side is the negative of this, reflected about $x = L/2$. If these two solutions do not decay sufficiently at $x = L/2$, the field will not be screened. We choose $n_B \approx 1/L^2$ as the value which begins to violate field screening since this will produce a small value in the exponent. The ion conservation condition $\int_0^L n\,dx = L$ is used to compare n_B to $1/L^2$. Using Eqs. (13) and (A9), this integral can be computed exactly. Assuming V sufficiently large (greater than a few thermal volts) and neglecting small terms, the result of this computation is that $V \approx 8\ln L$ when $n_B \approx 1/L^2$. Because the accumulation boundary concentrations in the $\hat{n} \to \infty$ limit are $e^{V/2}$, saturation will occur near the bias $V \approx 2\ln\hat{n}$. Comparing these two results leads to the inequality $\hat{n} < L^4$ for when the bias at which saturation occurs is less than that at which loss of field screening occurs in the diffuse limit.

5. Double layer potential drops and boundary fields

Eq. (A2) with $\phi_1 = \phi(0)$ and $\phi_2 = \phi(L)$ can be integrated exactly (see Eqs. (A3) and (A4)). Since $\phi_0' = \phi_L'$, the left side of Eq. (A2) is set to zero. The relations $\Delta\phi_- = -\phi(0)$ and $\Delta\phi_- + \Delta\phi_+ = V$ are then used to solve for the potential drops. For one-ion systems, the resultant equation can be solved exactly, leading to Eq. (23). The equation for the boundary field, Eq. (24), results from taking $\phi_1 = 0$ and $\phi_2 = \phi(0)$ (or $\phi_2 = \phi(L)$) in Eq. (A2). The remaining one-ion results are obtained from straightforward Taylor expansions of the exact results. The two-ion version of Eq. (A2) cannot be solved exactly; the saturation limit is investigated by assuming $e^{\phi(L)} \gg \hat{n}_a/n_B$ and $e^{-\phi(0)} \gg \hat{n}_c/n_B$ and then taking a Taylor expansion in these variables. The results given in Eqs. (29) and (30) additionally assume $n_B \approx 1$.

Appendix B: Asymptotic solution for θ

The steady-state electronic continuity equation, neglecting recombination and assuming $\beta = e^\phi$, is

$$0 = -F_e^{\text{inj}}\theta_e' + \lambda_F^{-1}\phi'\kappa_e e^\phi\left(1 - n_e(0) + F_e^{\text{inj}}\int_0^x \theta_e e^{-\phi}\,dx\right) \tag{B1}$$

Adding $F_e^{\text{inj}}\theta_e'$, dividing by $F_e^{\text{inj}}\phi'\kappa_e e^\phi$, differentiating, and then multiplying by $\phi'\kappa_e e^\phi$, this becomes

$$\theta_e'' - \left(\phi' + \frac{\phi''}{\phi'} + \frac{\kappa_e'}{\kappa_e}\right)\theta_e' - \lambda_F^{-1}\phi'\kappa_e\theta_e = 0 \tag{B2}$$

The asymptotic solution is now obtained by letting $\theta_e = e^{\Theta/\epsilon}$, where ϵ is a small parameter dependent on λ_F and $\Theta = \Theta_0 + \epsilon\Theta_1 + O(\epsilon^2)$. As $\epsilon \to 0$ and $\lambda_F \to 0$, the above equation becomes

$$\frac{\lambda_F}{\epsilon^2}\Theta_0'^2 \sim \phi'\kappa_e \tag{B3}$$

In the limit, in order for the left hand expression to remain nonzero and finite, we must take $\epsilon \propto \sqrt{\lambda_F}$. This now gives

$$\theta_e = \exp\left(-\frac{1}{\sqrt{\lambda_F}}\int_x^{x_1}\sqrt{\phi'\kappa_e}\,dx + O(1)\right) \tag{B4}$$

Computing more terms in the expansion (e.g. Θ_1) does not improve the result because the next term will cause divergence as x approaches x_1. Instead, an approximation is formed by requiring that $\theta_e = 1$ at $x = x_1$, or equivalently setting the $O(1)$ term to 0, giving Eq. (34).

Appendix C: The quasi-equilibrium condition

The problem is to phrase the inequality $\int_{x_\tau}^{x_-} e^{-\phi}\, dx < \int_{x_-}^{x_\zeta} e^{-\phi}\, dx$ in terms of λ_F. The second integral is approximated by $w_D e^{-\Delta\phi_-}$. The potential is approximated quadratically by writing Poisson's equation as $\phi'' \approx -\rho$ and letting w_i be the point where $\phi' = 0$; this gives $\phi \approx (\rho/2)(w_i^2 - (x - w_i^2))$ with $w_i = \sqrt{2\Delta\phi_-/\rho}$. The inequality has now become $\int_{x_\tau}^{w_i} e^{(\rho/2)(x-w_i)^2}\, dx < L$; evaluating this integral leads to

$$x_\tau > w_i - \sqrt{2/\rho}\, \mathrm{erfi}^{-1}\left(w_D\sqrt{2\rho/\pi}\right) \tag{C1}$$

where the right hand side is asymptotic to $w_i - \sqrt{\ln(\rho w_D^2 \ln(\rho w_D^2))/\rho}$ for large w_D. The asymptotic approximation $\theta \approx e^{-\int_x^{w_i}\sqrt{\phi'\kappa_e/\lambda_F}\, dx}$ and the condition $\theta''(x_\tau) = 0$ give an equation that can be solved for λ_F with some tedious computation; the above inequality on x_τ then leads to the result, Eq. (36).

Appendix D: Mixed ionic/electronic system

In treating the mixed ionic/electronic system, we assume that the double layer widths are negligible so that the width of the bulk region is approximately L.

1. Low-injection regime flux

If the electronic charges are injected in highly unequal proportions, or if recombination is negligible, the result is immediate.

Assuming high recombination, the profiles are approximated as linear until the point x_ζ where they meet, after which they are assumed to vanish. Then the width of the electron profile will be $x_\zeta - x_-$ and the width of the hole profile will be $x_+ - x_\zeta$. Because in this case the fluxes are equal and opposite, we have $F_{\mathrm{dev}} = \mu_e n_e(x_-)/(x_\zeta - x_-) = \mu_h n_h(x_+)/(x_+ - x_\zeta)$. The solution to this is

$$x_\zeta = x_- + (x_+ - x_-)\left(1 + \frac{\mu_h n_h(x_+)}{\mu_e n_e(x_-)}\right)^{-1} \tag{D1}$$

Letting $x_+ - x_- \approx L$, invoking quasi-equilibrium across the double layers to get $n_e(x_-) = \tilde{n}_e e^{\Delta\phi_-}$ and $n_h(x_+) = \tilde{n}_h e^{\Delta\phi_+}$, and substituting into either of the above expressions for F_{dev} gives the result, Eq. (37). Since this result holds both in the absence of recombination and in the limit of large recombination, we assume that it is a reasonable approximation in between as well.

2. Transition bias V_1

We define $u \equiv \phi'_L - \phi'_0 = \int_0^L n_e - n_h\, dx$ and find an expansion of the potential drops to first order in u. We define

$$y \equiv \frac{1}{2}\left(\phi_L'^2 - \phi_0'^2\right) = \int_0^L n_a - n_c + n_e - n_h\, d\phi \tag{D2}$$

It can be shown that $\int_0^L n_e - n_h\, d\phi$ is $O(u^2)$ and is therefore neglected. From above $y = u(\phi'_0 + u/2) = u\bar{\phi}'_0 + O(u^2)$, where $\bar{\phi}'_0$ is the value of ϕ'_0 when $u = 0$.

Solving Eq. (A2) for $\Delta\phi_{\mathrm{dep}}$ and expanding gives

$$\begin{aligned} \Delta\phi_{\mathrm{dep}} = {} & (1 - 1/\hat{n})V - \ln(r(\hat{n} - 1)) - u\bar{\phi}'_0/r\hat{n} \\ & + O(u^2 + e^{-(1-1/\hat{n})V + y/\hat{n}}) \end{aligned} \tag{D3}$$

where $r = 1 - e^{-V/\hat{n}}$. Now discarding the error term and approximating $u \approx (L/2)\tilde{n}e^{\Delta\phi_{\mathrm{dep}}}$ (linear carrier profile), this equation is solved to yield $u\bar{\phi}'_0/r\hat{n} \approx \mathrm{W}(L\tilde{n}\bar{\phi}'_0 e^{(1-1/\hat{n})V}/2r^2\tilde{n}(\tilde{n}-1))$. The transition is then considered to occur when the argument to this function is equal to 1 because it is near this point that $\Delta\phi_{\mathrm{dep}}$ begins to change its behavior. Using

$\bar{\phi}'_0 = \sqrt{2}\sqrt{(1-1/\hat{n})V - \ln(r(\hat{n}-1)) + \hat{n}\ln(1-1/\hat{n})}$, the bias at which this occurs can be obtained as an expression containing another W function; taking the asymptotic value $W(x) \sim \ln(x)$ gives

$$V_1 = \frac{1}{1-1/\hat{n}} \ln\left(\frac{2r^2\hat{n}(\hat{n}-1)}{L\tilde{n}}\right) \tag{D4}$$

In the saturation limit $(V \gg \hat{n})$, $r \sim 1$. In the diffuse limit, $r \sim V_1/\hat{n}$. Rather than solving again for V_1 in terms of W, it is much more convenient to estimate r by taking $V_1 \approx \ln(1/L\tilde{n})$.

The calculations for two-ion systems are done in exactly the same way, except that there is no r (since we neglect the diffuse limit). The final result again follows from taking $W \sim \ln$.

3. Space-charge regime flux

The flux is dominated by the majority carrier. For one-ion systems this is assumed to be the one injected at the depletion side; the flux is therefore $F_{\text{dev}} \approx \mu_{\text{maj}}\tilde{n}_{\text{maj}}e^{\Delta\phi_{\text{dep}}}/L$. Eq. (D3) with $r = 1$ is approximated using $W(x) \sim \ln x - \ln\ln x$ (the simpler approximation $W(x) \sim \ln x$ cannot be used because the important terms would cancel out) and the result substituted into the above approximation for F_{dev}; finally approximating $\bar{\phi}'_0 \approx \sqrt{(1-1/\hat{n})V}$ (Eq.(26)) yields Eq. (39). Again, the two-ion results follow from applying the same methods.

4. Transition bias V_2

The expression for V_2 is obtained by approximating $\Delta\phi$ across the double layer where the majority charges are injected as being fixed after reaching V_1, so that any additional bias beyond V_1 drops across the other double layer. Let $\Delta\phi_1$ be the majority double layer drop when $V = V_1$ (calculated from Eqs. (25), (29), and (38)). Approximating the carrier profiles as linear, we then solve for the bias V_2 at which the integrals of the carriers are equal. This gives

$$V_2 \approx 2\Delta\phi_1 + \ln\left(\sqrt{\frac{\mu_{\text{maj}}}{\mu_{\text{min}}}}\frac{\tilde{n}_{\text{maj}}}{\tilde{n}_{\text{min}}}\right) \tag{D5}$$

Eq. (40) then follows from substituting for $\Delta\phi_1$.

5. Bipolar regime flux

Equating integrals of linear carrier profiles using Eq. (D1) gives

$$n_e(x_-) = \sqrt{\frac{\mu_h}{\mu_e}}n_h(x_+) \tag{D6}$$

From this relation and the equalities $n_e(x_-) = \tilde{n}_e e^{\Delta\phi_-}$, $n_h(x_+) = \tilde{n}_h e^{\Delta\phi_+}$, and $\Delta\phi_+ = V - \Delta\phi_-$ (obtained by ignoring the bulk field) follows

$$\Delta\phi_- = \frac{V}{2} + \frac{1}{2}\ln\left(\sqrt{\frac{\mu_h}{\mu_e}}\frac{\tilde{n}_h}{\tilde{n}_e}\right) \tag{D7}$$

Substituting this into the flux expression and letting $w_B \approx L$ gives Eq. (41). Note also that (D6) implies that $x_\zeta \approx L/(1 + \sqrt{\mu_h/\mu_e})$, which is also valid in the high-injection regime.

6. Transition bias V_3 and high-injection regime fluxes

V_3 is defined as the minimum bias required to bring both the electronic carrier concentrations up to the equilibrium ionic concentration; hence, $V_3 = \ln(1/\tilde{n}_e\tilde{n}_h)$.

On both sides of a two-ion system, and on the accumulation side of a one-ion system, there will exist neutral layers in which $n_h = n_a$ and/or $n_e = n_c$, where the concentration profiles are approximately linear. We make use of a simple approximation to calculate the electronic fluxes in these regions. For example, taking $n_e = n_c$ and rearranging

the flux equation for n_c, we find that $-n'_e = \phi' n_e (1 - n_e/\hat{n}_c)$. The left hand side is the electronic diffusion flux, and the right hand side is nearly equal to the electronic drift flux in any region where $n_e \ll \hat{n}_c$. Therefore in such a region we have $F_e \approx -2n'_e$; in combination with assuming an approximately linear profile (an assumption well supported by simulation data), this allows us to calculate the electronic flux without calculating the field by writing $F_e \approx 2n_e(x_{\text{edge}})/w_e$ where x_{edge} is the edge of the linear (unsaturated) region and w_e is its width. In what follows, we will assume that this linear region extends all the way to the edge of the double layer; simulations show that this assumption is violated only for small values of $\hat{n}$.

a. One-ion systems

We will treat mobile anions. The device is split into four regions: the two double layers and two neutral regions. In the left-hand neutral region, the electrons are compensated by the immobile cations, so that $n_e = 1$ and $F_{\text{dev}} = F_e = \mu_e \phi'_e$, where ϕ'_e is the value of ϕ' in that region. In the right-hand region, $n_h \approx n_a$ and the profile is approximately linear, so $F_{\text{dev}} = -F_h \approx 2\mu_h n_h(x_+)/w_h$. We assume that all of the excess potential ΔV drops across the left-hand region (see Fig. 11); hence $\Delta V = \phi'_e w_e$. Because all of the anions are in the right-hand neutral layer, $n_h(x_+)w_h/2 = L$. Finally, let $w_e + w_h \approx L$. Eliminating w_e, w_h, $n_h(x_+)$, and ϕ'_e,

$$\Delta V = \frac{F_{\text{dev}}}{\mu_e}\left(L - 2\sqrt{\frac{\mu_h L}{F_{\text{dev}}}}\right) \tag{D8}$$

Eq. (43) follows from solving this equation for F_{dev} and identifying $\mu_1 = \mu_e$, $\mu_2 = \mu_h$.

b. Two-ion systems

In this case we assume that the excess bias ΔV is dropped across the junction region. The junction is assumed to be symmetric, with only electrons on its left side and only holes on its right. Ignoring diffusion flux in the junction, Poisson's equation becomes $\phi'' = F_{\text{dev}}/\mu_e \phi'$ on the left and $\phi'' = F_{\text{dev}}/\mu_h \phi'$ on the right. Solving these equations gives an expression for the junction potential,

$$\Delta V = \frac{\sqrt{F_{\text{dev}}}}{3}\left(\frac{1}{\sqrt{\mu_e}} + \frac{1}{\sqrt{\mu_h}}\right)w_J^{3/2} \tag{D9}$$

where w_J is the width of the junction. Now applying ionic charge conservation, $n_e(x_-)w_e/2 = n_h(x_+)w_h/2 = L$, and combining these with the flux expressions $F_{\text{dev}} = 2\mu_e n_e(x_-)/w_e = 2\mu_h n_h(x_+)/w_e$ along with the requirement that $w_e + w_J + w_h = L$ gives an expression for the junction width,

$$w_J = L\left(1 - 2\frac{\sqrt{\mu_e} + \sqrt{\mu_h}}{\sqrt{LF_{\text{dev}}}}\right) \tag{D10}$$

Setting $w_J = 0$ gives the flux at which the junction begins to form. Combining w_J with the above expression for ΔV permits one to solve for F_{dev}. While this equation can be solved exactly for F_{dev}, the solution involves the root of a cubic polynomial and is therefore too cumbersome to include here. Eq. (44) gives a Padé approximant of the solution about $\Delta V = 0$.

* lonergan@uoregon.edu

[1] Q. Pei, Y. Yang, G. Yu, C. Zhang, and A. Heeger, J. Am. Chem. Soc. **118**, 3922 (1996).

[2] D. Smith, J. Appl. Phys. **81**, 2869 (1997).

[3] I. Riess and D. Cahen, J. Appl. Phys. **82**, 3147 (1997).

[4] J.C. deMello, N. Tessler, S.C. Graham, and R.H. Friend, Phys. Rev. B **57**, 12951 (1998).

[5] J. Manzanares, H. Reiss, and A. Heeger, J. Phys. Chem. B **102**, 4327 (1998).

[6] M. Buda, G. Kalyuzhny, and A. Bard, J. Am. Chem. Soc. **124**, 6090 (2002).

[7] J.C. deMello, Phys. Rev. B **66**, 235210 (2002).

[8] D. Neher, J. Gruner, V. Cimrova, W. Schmidt, R. Rulkens, and U. Lauter, Polymers For Advanced Technologies **9**, 461 (1998).

[9] I. Riess, Solid State Ionics **136**, 1119 (2000).

[10] N. Armstrong, R. Wightman, and E. Gross, Ann. Rev. Phys. Chem. **52**, 391 (2001).

[11] L. Edman, in Iontronics, edited by J. Leger, M. Berggren, and S. Carter (CRC Press, Taylor and Francis Group, Boca Raton, Fl, 2011) Chap. 5, pp. 101–118.

[12] J. Gao, A. J. Heeger, I. H. Campbell, and D. L. Smith, Phys. Rev. B **59**, R2482 (1999).

[13] J.C. deMello, J.J.M. Halls, S.C. Graham, N. Tessler, and R.H. Friend, Phys. Rev. Lett. **85**, 421 (2000).

[14] J. C. deMello, Nat. Mater. **6**, 796 (2007).

[15] G. G. Malliaras, J. D. Slinker, J. A. DeFranco, M. J. Jaquith, W. R. Silveira, Y.-W. Zhong, J. M. Moran-Mirabal, H. G. Craighead, H. D. Abruna, and J. A. Marohn, Nat. Mater. **7**, 168 (2008).

[16] L. S. C. Pingree, D. B. Rodovsky, D. C. Coffey, G. P. Bartholomew, and D. S. Ginger, J. Am. Chem. Soc. **129**, 15903 (2007).

[17] P. Matyba, K. Maturova, M. Kemerink, N. D. Robinson, and L. Edman, Nat. Mater. **8**, 672 (2009).

[18] J. D. Slinker, J. A. DeFranco, M. J. Jaquith, W. R. Silveira, Y.-W. Zhong, J. M. Moran-Mirabal, H. G. Craighead, H. D. Abruna, J. A. Marohn, and G. G. Malliaras, Nat. Mater. **6**, 894 (2007).

[19] S. van Reenen, P. Matyba, A. Dzwilewski, R. A. J. Janssen, L. Edman, and M. Kemerink, J. Am. Chem. Soc. **132**, 13776 (2010).

[20] V. Cimrova, W. Schmidt, R. Rulkens, M. Schulze, W. Meyer, and D. Neher, Adv. Mater. **8**, 585 (1996).

[21] C. V. Hoven, A. Garcia, G. C. Bazan, and T.-Q. Nguyen, Adv. Mater. **20**, 3793 (2008).

[22] D. P. Stay, S. G. Robinson, and M. C. Lonergan, in Iontronics, edited by J. Leger, M. Berggren, and S. Carter (CRC Press, Taylor and Francis Group, Boca Raton, Fl, 2011).

[23] L. Edman, Electrochim. Acta **50**, 3878 (2005).

[24] H. Bassler, Phys. Status Solidi B **175**, 15 (1993).

[25] S. Rakhmanova and E. Conwell, App. Phys. Lett. **76**, 3822 (2000).

[26] S. Druger, A. Nitzan, and M. Ratner, J. Chem. Phys. **79**, 3133 (1983).

[27] W. Dieterich, O. Durr, P. Pendzig, A. Bunde, and A. Nitzan, Physica A **266**, 229 (1999).

[28] J. Crank, The mathematics of diffusion (Clarendon Press, Oxford, [Eng], 1975).

[29] J.C. deMello, J. Comput. Phys. **181**, 564 (2002).

[30] C. B. Duke, Tunneling in solids (Academic Press, New York, 1969).

[31] R. Tsu and L. Esaki, App. Phys. Lett. **22**, 562 (1973).

[32] R. J. D. Miller, Surface electron transfer processes (VCH, New York, 1995).

[33] E. H. Rhoderick and R. H. Williams, Metal-semiconductor contacts (Clarendon Press ; Oxford University Press, Oxford [England]; New York, 1988).

[34] W. A. Harrison, Phys. Rev. **123**, 85 (1961).

[35] M. Langevin, Ann. Chim. Phys. **28**, 433 (1903).

[36] See epaps document no. ?? for details further detail on the simulation methods. For more information on epaps, see http://www.aip.org/pubservs/epaps.html.

[37] M. Eigen and E. Wicke, J. Phys. Chem. **58**, 702 (1954).

[38] A. J. Bard and L. R. Faulkner, Electrochemical methods : fundamentals and applications (Wiley, New York, 1980).

[39] I. Riess, Solid State Ionics **69**, 43 (1994).

[40] C. Crowell and S. Sze, Solid-State Electronics **9**, 1035 (1966).

[41] P. Davids, S. Kogan, I. Parker, and D. Smith, App. Phys. Lett. **69**, 2270 (1996).

[42] R. Buck, J. Phys. Chem. **93**, 6212 (1989).

[43] J. deMello, N. Tessler, S. Graham, X. Li, A. Holmes, and R. Friend, Synthetic Metals **85**, 1277 (1997).

[44] T. Johansson, W. Mammo, M. R. Andersson, and O. Inganas, Chemistry of Materials **11**, 3133 (1999).

[45] M. Sampietro, R. Sotgiu, F. Wenzl, L. Holzer, S. Tasch, and G. Leising, Phys. Rev. B **61**, 266 (2000).

[46] R. Marcilla, D. Mecerreyes, G. Winroth, S. Brovelli, M. d. M. R. Yebra, and F. Cacialli, App. Phys. Lett. **96** (2010).

[47] F. Pichot, C. J. Bloom, L. S. Rider, and C. M. Elliott, J. Phys. Chem. B **102**, 3523 (1998).

[48] C. H. W. Cheng, F. Lin, and M. C. Lonergan, J. Phys. Chem. B **109**, 10168 (2005).

[49] M. Lampert, Phys. Rev. B **103**, 1648 (1956).

[50] J. Fang, P. Matyba, N. D. Robinson, and L. Edman, J. Am. Chem. Soc. **130**, 4562 (2008).